© 2016. Published by The Company of Biologists Ltd | Journal of Cell Science (2016) 129, 3756-3769 doi:10.1242/jcs.187336

RESEARCH ARTICLE

Direct interaction between exocyst and Wave complexes promotes cell protrusions and motility

Marco Biondini[1,2], Amel Sadou-Dubourgnoux[1,2], Perrine Paul-Gilloteaux[1,3], Giulia Zago[1,2], Melis D. Arslanhan[1,2], François Waharte[1,3], Etienne Formstecher[4], Maud Hertzog[5], Jinchao Yu[6], Raphael Guerois[6], Alexis Gautreau[7], Giorgio Scita[8], Jacques Camonis[1,2] and Maria Carla Parrini[1,2,*]

ABSTRACT

Coordination between membrane trafficking and actin polymerization is fundamental in cell migration, but a dynamic view of the underlying molecular mechanisms is still missing. The Rac1 GTPase controls actin polymerization at protrusions by interacting with its effector, the Wave regulatory complex (WRC). The exocyst complex, which functions in polarized exocytosis, has been involved in the regulation of cell motility. Here, we show a physical and functional connection between exocyst and WRC. Purified components of exocyst and WRC directly associate *in vitro*, and interactions interfaces are identified. The exocyst–WRC interaction is confirmed in cells by co-immunoprecipitation and is shown to occur independently of the Arp2/3 complex. Disruption of the exocyst–WRC interaction leads to impaired migration. By using time-lapse microscopy coupled to image correlation analysis, we visualized the trafficking of the WRC towards the front of the cell in nascent protrusions. The exocyst is necessary for WRC recruitment at the leading edge and for resulting cell edge movements. This direct link between the exocyst and WRC provides a new mechanistic insight into the spatio-temporal regulation of cell migration.

KEY WORDS: Wave, Exocyst, Motility, Ral

INTRODUCTION

Cell motility is involved in a large variety of biological phenomena, from embryogenesis to cancer progression. Different molecules and pathways have been linked to cell migration, but an integrated and dynamic view of their interplay in the spatio-temporal space of the cell is still missing (Anitei et al., 2010; Ridley et al., 2003; Welf and Haugh, 2011).

In motile cells, the Rac1 GTPase drives the formation of the actin polymerization network at front protrusions by interacting with its effector, the Wave regulatory complex (WRC). The WRC is composed of a Wave protein [Wave1, Wave2 or Wave3, also known as WASF1, WASF2 and WASF3, respectively], Abi (Abi1, Abi2 or Abi3), Nap1 (also known as NCKAP1), Cyfip1 (also called Sra1 or Pir121) and HSPC300 (also called Brick1). These five proteins constitutively and strongly associate in the cell to form the pentameric heterocomplex (Eden et al., 2002; Gautreau et al., 2004). The WRC is intrinsically inactive (Derivery et al., 2009; Ismail et al., 2009), and at least three signals are required to fully stimulate Wave activity: phosphorylation by various kinases, including Abl and Erk proteins (Leng et al., 2005; Mendoza et al., 2011); interaction with Rac1-GTP (through the Cyfip1 subunit); and binding of phosphatidylinositol 3-phosphate phospholipids (Derivery and Gautreau, 2010; Lebensohn and Kirschner, 2009). The C-terminal verprolin homology, connector, acidic region (VCA) of the Wave subunit is sequestered according to the crystal structure of inactive WRC (Chen et al., 2010). Upon activation, the VCA domain is exposed and becomes available to bind to the Arp2/3 complex (which comprises seven subunits, two of which are ARPC2 and ARPC3) and to stimulate the nucleation of new actin filaments. Although the biochemical mechanisms of WRC activation have been largely clarified, very little is known about the spatio-temporal regulation of WRC localization.

Various studies, including those of our laboratory, have identified a migration-regulating pathway that emanates from the RalB GTPase and its downstream effector, the exocyst complex (Lim et al., 2006; Oxford et al., 2005; Rossé et al., 2006), which comprises eight subunits in yeast (Sec3, Sec5, Sec6, Sec8, Sec10, Sec15, Exo70 and Exo84). The exocyst, evolutionarily conserved from yeast to mammals, is required for polarized exocytosis – it mediates the targeting and tethering of post-Golgi secretory vesicles to specific membrane sites (He and Guo, 2009). Intracellular membrane trafficking, with its cycles of endocytosis and exocytosis, is a master organizer of signaling pathways and plays a crucial role in trafficking specific molecules to the right place at the right time (Scita and Di Fiore, 2010). With regard to cell motility, exocyst has been proposed to promote the transport and recruitment of regulatory molecules to the leading edge of migrating cells. For example, the RacGAP SH3BP1 binds to exocyst to be transported to the front of the cell, where it inactivates Rac1 (Parrini et al., 2011); similarly, the RhoGEF GEF-H1 interacts with exocyst possibly to be delivered to specific sites, where it activates RhoA (Biondini et al., 2015; Pathak et al., 2012).

In this work, by searching for new connections between the Rac1–WRC and RalB–exocyst pathways in a series of screens performed in the laboratory, we discovered a much unexpected link – the WRC and exocyst directly interact. Here, we report the biochemical characterization of this interaction and its functional relevance for cell motility. This finding provides a new molecular basis underlying the spatio-temporal coordination of membrane trafficking and actin polymerization in motile cells.

[1]Institut Curie, Centre de Recherche, Paris Sciences et Lettres Research University, Paris 75005, France. [2]ART group, Inserm U830, Paris 75005, France. [3]Cell and Tissue Imaging Facility (PICT-IBiSA), CNRS UMR 144, Paris 75005, France. [4]Hybrigenics, Paris 75014, France. [5]Laboratoire de Microbiologie et Génétique Moléculaire, CNRS UMR 5100, Université Paul Sabatier, Toulouse 31062, France. [6]Institute for Integrative Biology of the Cell (I2BC), CEA, CNRS, University Paris-Saclay, CEA-Saclay, Gif-sur-Yvette 91191. [7]Laboratoire de Biochimie Ecole Polytechnique, CNRS UMR7654, Palaiseau Cedex 91128, France. [8]IFOM, Fondazione Istituto FIRC di Oncologia Molecolare and Dipartimento di Scienze della Salute, Università degli Studi di Milano, Milan 20139, Italy.

*Author for correspondence (maria-carla.parrini@curie.fr)

M.C.P., 0000-0002-7082-9792

Received 15 February 2016; Accepted 16 August 2016

Journal of Cell Science

Journal of Cell Science (2016) 129, 3756-3769 doi:10.1242/jcs.187336

RESULTS

Exocyst and WRC directly interact

A series of yeast two-hybrid screens aimed at identifying human proteins interacting with the human exocyst indicated that exocyst and WRC might associate through two points of contact (Fig. 1A). In particular, the Abi1 and Abi2 subunits of the WRC were recovered from yeast two-hybrid screens with full-length human EXOC7 variant 1 (the homolog of *Saccharomyces cerevisiae* Exo70). A second WRC subunit, Cyfip1, was found in screens performed with human EXOC3 (the homolog of *S. cerevisiae* Sec6; fragment comprising residues 297–745). Yeast nomenclature has been used for human exocyst proteins herein. The deduced minimal Exo70-interacting domain of Abi1 and Abi2 corresponded to residues 37–188 (total length of Abi proteins is 329–513 residues, depending on the isoform). By contrast, the minimal Sec6-interacting domain of human Cyfip1 (1253 residues) comprised the residues 326–508, which overlap with the Cyfip1 region that binds to Rac1-GTP (Kobayashi et al., 1998) (Fig. 1B).

To validate these interactions biochemically, we performed *in vitro* binding assays with purified proteins. Exo70 and Sec6 were purified from *E. coli* as GST-fusion products, whereas Abi1 was purified from insect cells. By using GST pulldown assays, we found that GST–Exo70 efficiently bound to purified Abi1 to extent similar to EPS8, a well-characterized Abi1-interacting protein (Disanza et al., 2004), demonstrating the direct interaction between Exo70 and Abi1 (Fig. 1C). Such a simple strategy could not be applied to the Sec6–Cyfip1 interaction because isolated Cyfip1 is unstable. Because Cyfip1 folding can be stabilized by the association to Nap1, we co-overexpressed in HEK293 cells Flag-tagged Nap1 together with Myc-tagged Cyfip1 and co-isolated a bi-molecular Nap1–Cyfip1 complex by using anti-Flag immunoprecipitation, as previously reported (Innocenti et al., 2004). The bead-bound Nap1–Cyfip1 complex was incubated with purified GST–Sec6 and GST–Exo70 (Fig. 1D) – Sec6 (lane 8) but not Exo70 (lane 7) associated with Nap1–Cyfip1; neither Exo70 nor Sec6 associated with Nap1 alone (lanes 5 and 6) nor with a control unrelated Flag–MEK1 (human MAP2K1) fusion (lanes 3 and 4). These results indicate that Cyfip1, but not Nap1, interacts with Sec6 but not with Exo70, confirming the two-hybrid analysis findings. Consistently, the whole pentameric WRC binds *in vitro* to both GST–Sec6 (through Cyfip1) and GST–Exo70 (through Abi1) but not to GST alone (Fig. S1A and B).

Our two-hybrid data indicate that the region of Cyfip1that binds to Sec6 overlaps with the site in Cyfip1 required to bind to active Rac1 (Kobayashi et al., 1998), suggesting that active Rac1 might compete with exocyst for binding to WRC. Competition experiments using purified proteins, however, did not support this possibility. Indeed, soluble GST–Sec6 bound to immobilized WRC even in the presence of a large molar excess of soluble active Rac1 (Q61L mutant), indicating that active Rac1 cannot prevent the association of WRC with Sec6, at least *in vitro*, and suggesting the possible existence of a super-complex comprising exocyst–WRC–Rac1-GTP *in vivo* (Fig. 1E).

Exocyst and WRC associate in cells

To study WRC and exocyst complexes in cells, we used HEK293 cells stably expressing tagged human subunits (Flag–HA–Cyfip1 and Flag–HA–Abi1 for WRC; V5–Sec6 and V5–Sec5 for exocyst). The level of expression of exogenous proteins was comparable to that of endogenous ones. We confirmed the previously reported observation (Derivery et al., 2009) that tagged Cyfip1 and Abi1 replace the endogenous subunits in the WRC (Fig. S1A). Moreover, we observed that, in the presence of V5–Sec6, endogenous Sec6 is no longer detectable in the whole lysates, suggesting that a similar molecular replacement mechanism occurs for the exocyst complex (Fig. 2B).

When immunoprecipitations of Flag were performed on lysates from cell lines expressing Flag–HA–Cyfip1, the whole WRC was retrieved as expected – bands representing Cyfip1, Nap1, Wave2 and Abi1 appeared in an approximately stoichiometric ratio, according to the quantification on a Ponceau-Red-stained gel (note that Brick1 runs off standard gels because of its small size). Importantly, endogenous Exo70 and Sec8 co-immunoprecipitated with the WRC from Flag–HA–Cyfip1-expressing cells, but not from control cells expressing Flag–HA tag only (Fig. 2A). However, in the immunoprecipitates, we could not detect Sec6, the direct interactor of Cyfip1. This is likely to be due to the weak sensitivity of the available antibodies against Sec6. Endogenous Exo70, the direct interactor of Abi1, was also found to be associated with the WRC isolated from Flag–HA–Abi1-expressing cells (Fig. S1C).

In parallel, immunoprecipitations of V5 were performed on lysates from cell lines expressing V5–Sec6. The stoichiometry of the retrieved exocyst complex was not equimolar, the Sec6 subunit being in excess with respect to other components. This was not surprising considering the dynamic nature of this complex. All exocyst subunits for which antibodies were available (Sec5, Sec6, Sec8, Exo70, Exo84) were present in the immunoprecipitates. Endogenous Cyfip1 protein specifically co-immunoprecipitated with this Sec6-enriched exocyst complex (Fig. 2B), which is consistent with the existence of a Sec6–Cyfip1 interaction in cells. In addition, we also specifically detected Wave2 and Nap1 in the exocyst precipitates from both V5–Sec6- and V5–Sec5-expressing cells (Fig. 2C). In conclusion, no matter which subunit of WRC (Cyfip1 or Abi1) or exocyst (Sec6 or Sec5) was precipitated, components of the other complex were detected (Sec8 and Exo70 precipitated with WRC subunits; and Cyfip1, Wave2 and Nap1 precipitated with exocyst components), suggesting that assembly occurs between the whole complexes and not simply between isolated subunits.

The Arp2/3 complex is a shared interacting complex of both WRC and Exo70. Indeed, W. Guo and colleagues have shown that Exo70 directly binds to the ARPC1 subunit of the Arp2/3 complex, and promotes actin branching by acting as a kinetic activator of Arp2/3 (Liu et al., 2012; Zuo et al., 2006). To directly assess a possible involvement of Arp2/3 as bridge in mediating the WRC–exocyst interaction, we treated our cells with small interfering (si)RNAs targeting the crucial subunit ARPC2, a condition known to induce degradation of the entire Arp2/3 complex (Abella et al., 2016). We verified in particular the depletion of the subunits ARPC1A and ARPC1B, which interact with Exo70. Under these conditions, we still observed co-precipitation of Exo70 upon precipitation of the WRC, providing evidence against the notion that Arp2/3 mediates the interaction between WRC and exocyst (Fig. 2D).

We found that our cells mainly expressed the Exo70 isoform 2 [also known as the mesenchymal (M) variant, denoted Exo70-2M] (Fig. S1D), which has been reported to bind to Arp2/3 (Lu et al., 2013). On the contrary, the Exo70 isoform 5 [also known as the epithelial variant (E), denoted Exo70-5E], carrying a 23-amino-acid insertion conferred by alternative splicing, does not bind to Arp2/3 (Lu et al., 2013). We expressed GFP-fused Exo70-5E and Exo70-2M in the HEK293 Flag–HA–Abi1-expressing cell line. Both isoforms were found to be associated with the WRC that could by immunoprecipitated with an antibody against Flag (Fig. S1E). The observation that Exo70-5E, which cannot bind to Arp2/3, is still

Journal of Cell Science (2016) 129, 3756-3769 doi:10.1242/jcs.187336

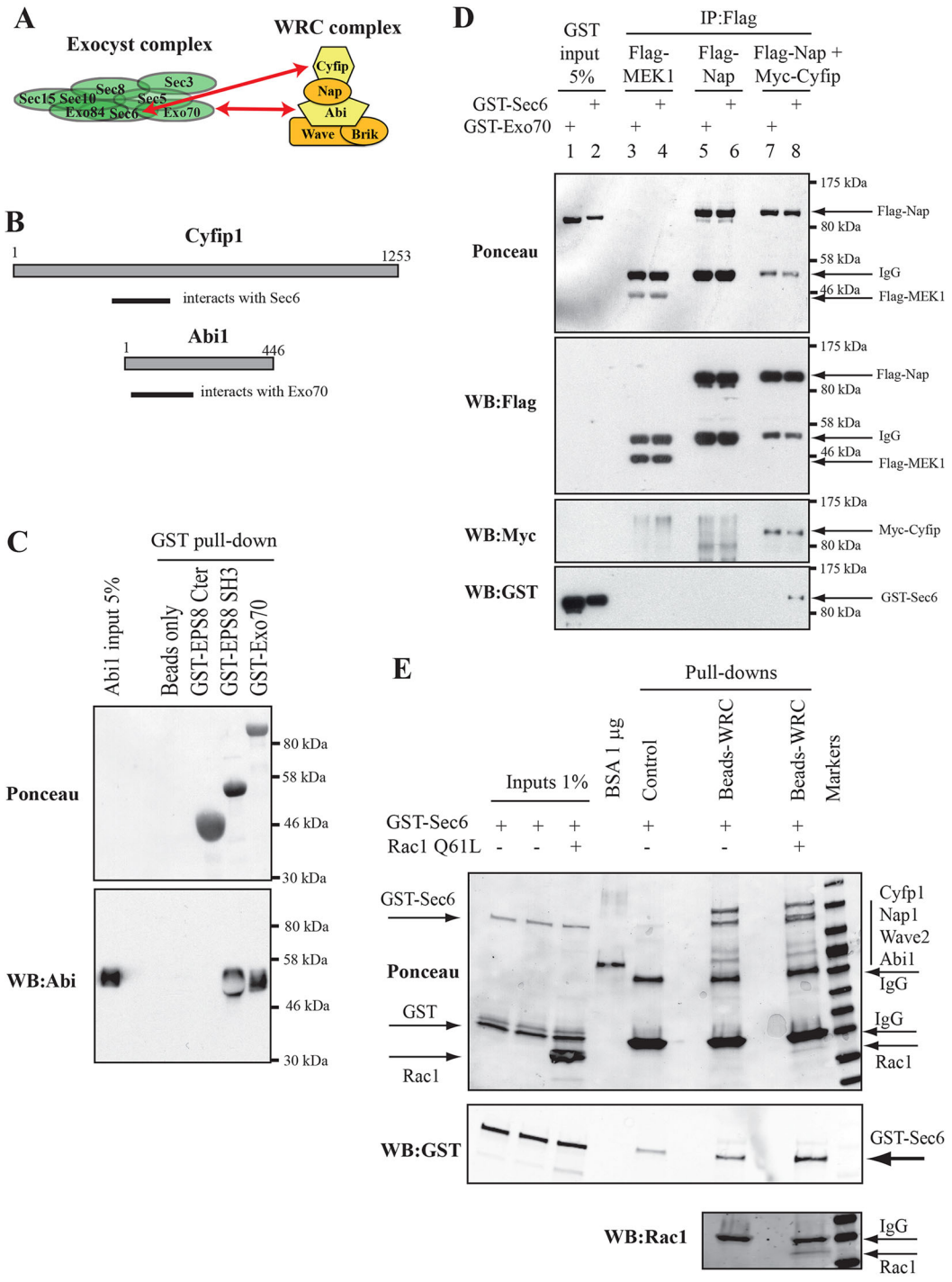

Fig. 1. Subunits of WRC and exocyst complexes directly interact *in vitro*. (A) Schematic representation of WRC and exocyst complexes. The newly identified interactions, Exo70 with Abi1 or Abi2, and Sec6 with Cyfip1 (Cyfip), are indicated by the red arrows. (B) Summary of the two-hybrid screen results. (C) GST–Exo70 directly interacts with Abi1 *in vitro*. Abi1 protein, purified from insect cells, was incubated either with beads alone or with beads coupled to GST–EPS8-Cter (residues 648–821) (negative control), to GST–EPS8-SH3 (residues 535–821) (positive control) or to GST–Exo70. After washing, pulled-down proteins were loaded onto an SDS gel, transferred to membrane and stained with Ponceau Red (upper panel) or with antibodies against Abi1 (lower panel). The white shadow in the Abi western blot (WB) is due to the large amount of GST–EPS8-SH3, which has a molecular weight very similar to that of Abi1. (D) GST–Sec6 directly interacts with Cyfip1 *in vitro*. GST–Exo70 and GST–Sec6 proteins were produced in *E. coli*, affinity-purified and eluted from beads with glutathione. Flag–MEK1 alone (negative control), Flag–Nap1 alone and Flag–Nap1 together with Myc–Cyfip1 were expressed in HEK293 human cells. Flag fusions were immunoprecipitated with beads coupled to anti-Flag antibodies. The beads were then incubated with GST–Sec6 or GST–Exo70. After washing, pulled-down proteins were stained with Ponceau Red and with anti-Flag, anti-Myc or anti-GST antibodies. (E) Active Rac1 does not prevent Sec6 from binding to WRC. The WRC was purified by immunoprecipitation with anti-Flag antibodies from HEK293 human cells stably expressing Flag–HA–Abi1. The concentration of beads that bound to WRC was approximately 0.025 µM, as estimated from the gel using 1 µg of bovine serum albumin (BSA) as reference. The WRC-bound beads were incubated for 2 h with GST–Sec6 (1 µM), without or with Rac1-Q61L (50 µM – i.e. 2000-fold molar excess with respect to WRC). After washing, the proteins that were retained on the beads were analyzed by SDS-PAGE. Under these conditions, Rac1-Q61L appeared to bind to WRC with close stoichiometry, considering that the Rac1 molecular mass is approximately one-sixth of that of Cyfip1. This Rac1–WRC complex still efficiently interacts with Sec6.

Journal of Cell Science (2016) 129, 3756-3769 doi:10.1242/jcs.187336

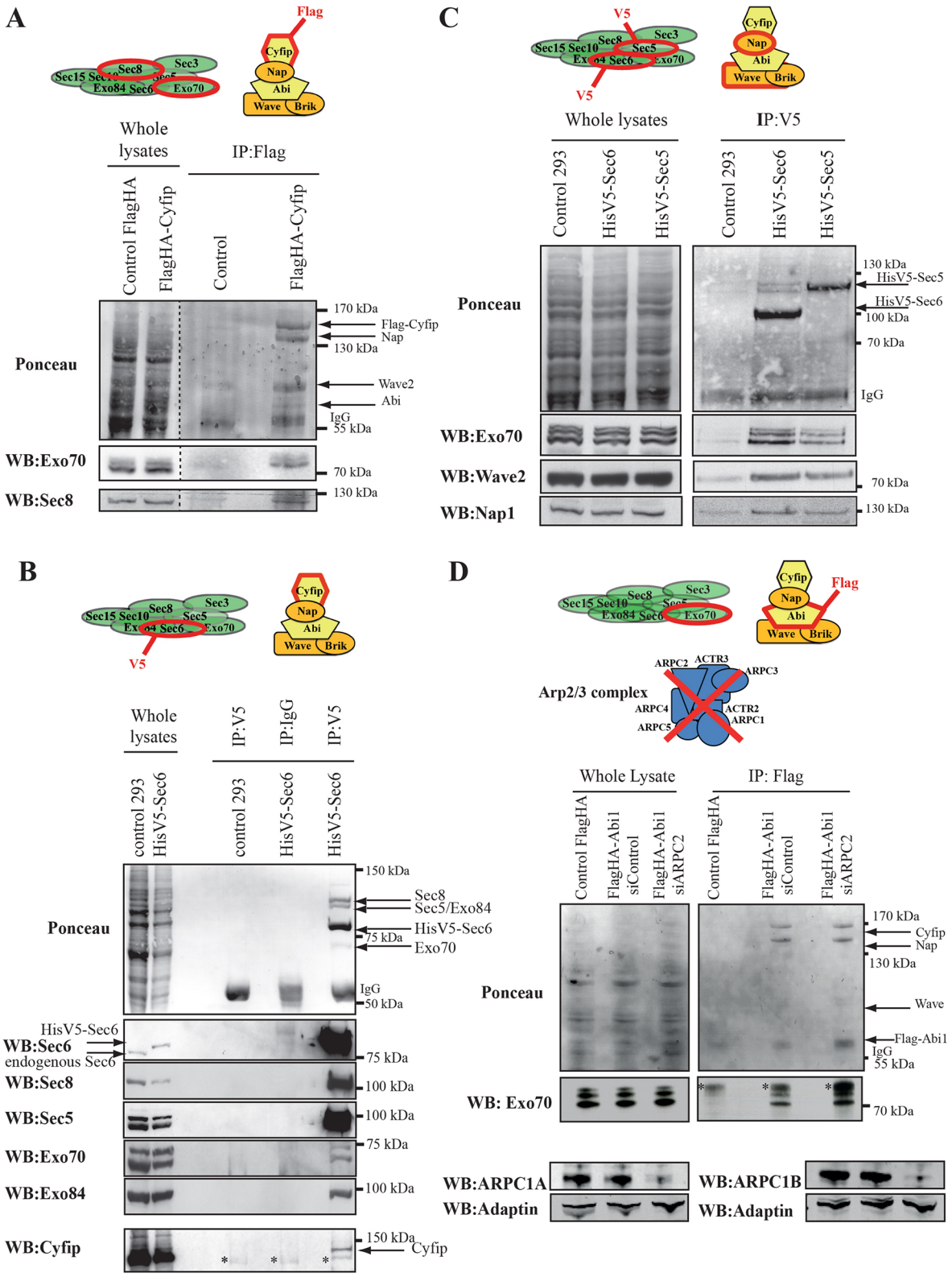

Fig. 2. See next page for legend.

able to bind to WRC, indicates that the interaction between Exo70 and WRC occurs independently of the interaction between Exo70 and Arp2/3.

We reasoned that the exocyst and WRC might interact locally and/or transiently, possibly during cell migration. Hence, we focused our investigation on motile cells, using HEK-HT cells (which ectopically express hTERT and large and small T-antigen) as motility model (Hahn et al., 1999). Randomly moving HEK-HT cells were fixed and co-stained with antibodies against Wave2 and against Exo70 or Sec6. All three proteins were found at cell

Journal of Cell Science (2016) 129, 3756-3769 doi:10.1242/jcs.187336

Fig. 2. Exocyst and WRC associate in cells. (A) WRC associates with endogenous Exo70 and Sec8. In HEK293 human cells that stably expressed a Flag–HA–Cyfip1 construct or Flag–HA only as negative control, the whole WRC was immunoprecipitated (IP) with anti-Flag antibodies, as shown by Ponceau Red staining (upper panel). A fraction of endogenous Exo70 and Sec8 co-precipitated with the WRC (lower panel). (B) Sec6-enriched exocyst complex associates with endogenous Cyfip1 (Cyfip). In HEK293 human cells that stably expressed a His–V5–Sec6 construct, the exocyst complex was immunoprecipitated with anti-V5 antibodies, as shown by the Ponceau Red staining (upper panel) and the detection of Sec6, Sec8, Sec5, Exo70 and Exo84 (middle panel). Negative controls were performed – immunoprecipitation with anti-V5 antibodies in parental HEK293 cells and immunoprecipitation with unrelated IgG in His–V5–Sec6-expressing HEK293 cells. A fraction of endogenous Cyfip1 co-precipitated with the exocyst complex (lower panel). *Non-specific bands. (C) Sec6-enriched and Sec5-enriched exocyst complexes associate with endogenous Wave2 and Nap1. In HEK293 human cells that stably expressed His–V5–Sec6 or His–V5–Sec5 constructs, the exocyst complex was immunoprecipitated with anti-V5 antibodies, as shown by the Ponceau-Red staining (upper panel) and the detection of Exo70 (middle panel). As negative control, we immunoprecipitated V5 from parental HEK293 cells. A fraction of endogenous Wave2 and Nap1 co-precipitated with the exocyst complex (lower panels). (D) Depletion of the Arp2/3 complex does not impair WRC association with Exo70. Flag–HA–Abi1-expressing HEK293 human cells were treated with control siRNA (siControl) or siRNA against ARPC2 (siARPC2). The whole WRC was immunoprecipitated with anti-Flag antibodies. As negative control, we immunoprecipitated Flag from HEK293 cells expressing Flag–HA only. A fraction of endogenous Exo70 co-precipitated with the WRC, both without and with silencing of ARPC2. ARPC2 silencing leads to degradation of the entire Arp2/3 complex (Abella et al., 2016); depletion of ARPC1A and ARPC1B subunits was verified by western blotting (WB) (lower panels). Adaptin was detected as loading control. *Non-specific bands. Sec5/Exo84, Sec5 and Exo84, which are indistinguishable by staining with Ponceau.

protrusions in agreement with previous reports (Nozumi et al., 2003; Rossé et al., 2006; Zuo et al., 2006), with extensive apparent overlap, as shown by confocal microscopy analysis (Fig. 3). However, their patterns were different – Wave2 was clearly located at the very edge of lamellipodia, with a sharp and continuous signal; the front-edge staining of Sec6 and Exo70 appeared, instead, blurred and discontinuous. Finally, almost 50% of the protrusions positive for Wave2 staining were devoid of Exo70 or Sec6 (n=35 protrusions from 21 cells). In Fig. 3, we show representative fluorescence intensity plots of both exocyst and WRC overlapping staining (region a) and WRC-only staining (region b).

These data suggest that the active WRC is not bound in a compulsory manner to the exocyst at the edge. Because Rac1 activates the WRC by interacting with Cyfip1, it is possible that WRC is retained by Rac1, whereas the exocyst recycles in the cytosol.

Mapping of the Exo70–Abi interaction surface

To identify the Exo70–Abi interaction surface, we co-overexpressed wild-type and deletion mutants of GFP-fused Abi1 and Exo70–HA constructs, and we performed immunoprecipitations for GFP.

For Abi proteins, we found that the full-length, but not a mutant lacking the N-terminal domain of Abi1 (residues 1–145), co-precipitated with Exo70–HA. The N-terminal domain of Abi2, which is nearly identical to that of Abi1, was sufficient for a very weak interaction (Fig. 4A). This indicates that the N-terminal domain of Abi proteins is necessary and even sufficient to some extent to drive the interaction between Exo70 and Abi, consistent with the two-hybrid data.

To further investigate how the Abi N-terminal could interact with Exo70 in the context of the WRC assembly, the conservation of residues accessible at the surface of Abi1 and Abi2 in WRC was analyzed using the Rate4Site algorithm (http://www.tau.ac.il/~itaymay/cp/rate4site.html) applied on a multiple sequence alignment of 150 homologs of Abi1 and Abi2 in animals (Pupko et al., 2002). A conserved surface patch could be delineated between the helices of Abi1 spanning the regions comprising residues 18–36 and 47–65 (Fig. 4B). At the center of this patch, the residue Q56 is exposed and nearly invariant. We generated the mutation Q56A together with two other mutations, Y32E and Y63E, corresponding to exposed and conserved aromatic residues at the edge of the conserved patch. Only the Q56A mutation substantially decreased the interaction with Exo70 (Fig. 4C), showing that this exposed position plays a key role in bridging WRC and Exo70.

For Exo70, the N-terminal Exo70 moiety (residues 1–414), but not the C-terminal Exo70 moiety (residues 415–C-terminus), binds to full-length Abi1. Exo70 has an N-terminal coiled-coil motif as predicted using the PCOILS program (https://toolkit.tuebingen.mpg.de/pcoils) (Lupas et al., 1991). The deletion of this N-terminal coiled-coil motif (residues 1–84; Exo70-Δ84) abolished the binding to Abi1 (Fig. 4D). A very similar sequence (residues 1–75) has been reported to be necessary for Exo70 dimerization (Zhao et al., 2013).

Exocyst–WRC association contributes to cell migration

We used the Exo70-Δ84 mutant, which is deficient in binding to Abi1, to investigate the functional consequence of impairing exocyst–WRC association during motility. In HEK-HT cells, as expected (Zuo et al., 2006), the depletion of Exo70 inhibited the speed of cell motility. This phenotype was rescued by re-expression of wild-type Exo70 but not by the re-expression of the Exo70-Δ84 mutant (Fig. 5A and B). Thus, the N-terminal region of Exo70 is necessary for efficient cell motility, in agreement with a previous report that used an Exo70-Δ75 mutant (Zhao et al., 2013). Importantly, the depletion of the N-terminus of Exo70 (residues 1–75) was not shown to affect exocyst assembly nor its function in exocytosis (Zhao et al., 2013). Therefore, the motility defect of cells expressing N-terminal truncated Exo70 mutants (Δ84 or Δ75) is not due to a general loss-of-function of the entire exocyst complex. Our findings are consistent with the interpretation that the depletion of the Exo70 N-terminal region inhibits cell migration at least in part because it impairs the exocyst–WRC association, supporting a role for exocyst–WRC association during cell migration.

Identification of a forward flow of WRC

We reasoned that the requirement of an exocyst–WRC association for efficient migration might underlie a function of exocyst in the dynamics of WRC localization. To directly visualize the spatio-temporal dynamics of the WRC in motile HEK-HT cells, we exogenously expressed a GFP–Abi1 fusion. Importantly, the expression level of GFP–Abi1 was kept as low as possible to favor its incorporation into the endogenous WRC. With such a precaution, by confocal spinning-disc fast-acquisition imaging, we clearly observed a sharp recruitment of GFP–Abi1 at the edge of nascent and expanding protrusions (Fig. 6A; Movie 1), as previously reported (Stradal et al., 2001).

In regions just behind the active edges, WRC live localization appeared like a dense meshwork of fluorescent highly dynamic cytosolic dots. As originally reported using a single-molecule imaging approach (Millius et al., 2012), we also observed rare events of WRC retrograde motion, which we manually tracked to find a median speed of 0.161 µm/s (s.d.=0.036, n=13 dots from five cells); this is consistent with the notion that a portion of the WRC population is recycled through incorporation into the actin network, undergoing retrograde flow (Millius et al., 2012). However, most of the movements of these Abi-positive dots at protrusions were not

Journal of Cell Science (2016) 129, 3756-3769 doi:10.1242/jcs.187336

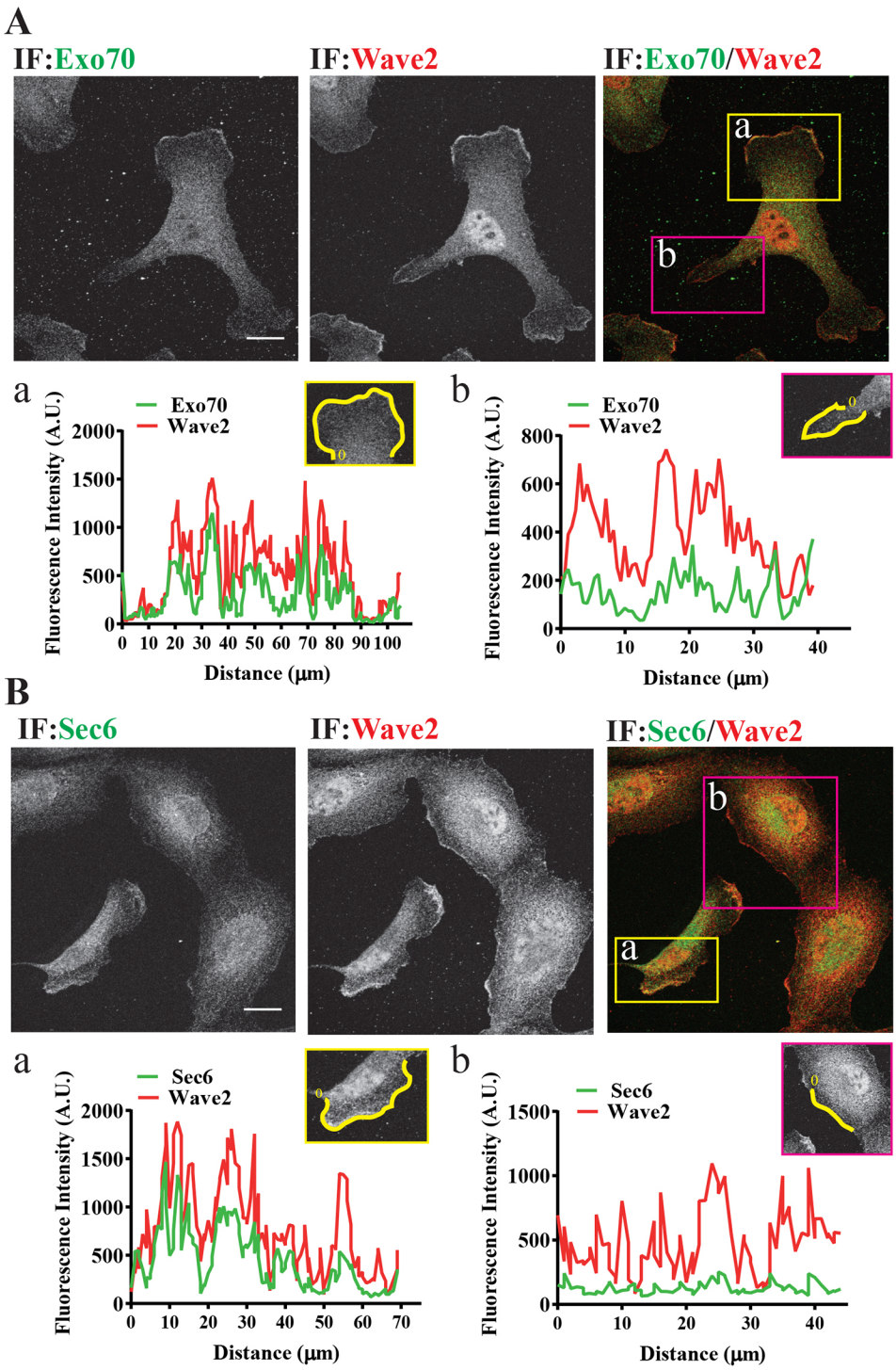

Fig. 3. Exo70 and Sec6 staining partially overlaps with Wave2 staining at the leading edge of randomly moving cells. (A) Representative confocal images of motile HEK-HT cells co-stained for Exo70 and Wave2. For the two indicated protrusive regions (region a and region b), the fluorescence intensity values for both Exo70 (green) and Wave2 (red) along the cell edge were plotted in graphs. The yellow line in the inserts shows the measured cell edge (0 indicates the starting point of measurement). Scale bar: 20 µm. (B) Representative confocal images of motile HEK-HT cells co-stained for Sec6 and Wave2. Quantifications were performed as described in panel A. Scale bar: 20 µm. IF, immunofluorescence.

trackable because of their high density and their rapid movements. Therefore, we took advantage of the spatio-temporal image correlation spectroscopy technique (STICS) (Hebert et al., 2005). STICS allows measurement of both diffusion coefficients and velocity vectors (magnitude and direction), or 'molecular flow', for fluorescently labeled proteins in living cells through space–time correlation functions.

We applied STICS analysis to the front portions of motile cells expressing GFP–Abi1. Fig. 6B shows an example of estimation, both in space and in time, of Abi1 flow by STICS analysis in a representative cell. The displacement of the peak of the spatial autocorrelation function (ACF) indicates both the direction of flow and its magnitude (Hebert et al., 2005).

The velocity of the molecular WRC flow was in the range 0.001–0.09 µm/s, with a median of 0.0215 µm/s (s.d.=0.023, n=82 measurements from 21 regions of interest at various time intervals, from eight independent cells). These measured flows were not simply due to cytosolic motions because the same analysis on control cells (expressing GFP) only very rarely could detect a molecular flow that was always very slow (median 0.005 µm/s, s.d.=0.005, n=22 measurements from six regions of interest from three control GFP cells). Globally, the WRC flows did not show a

Journal of Cell Science (2016) 129, 3756-3769 doi:10.1242/jcs.187336

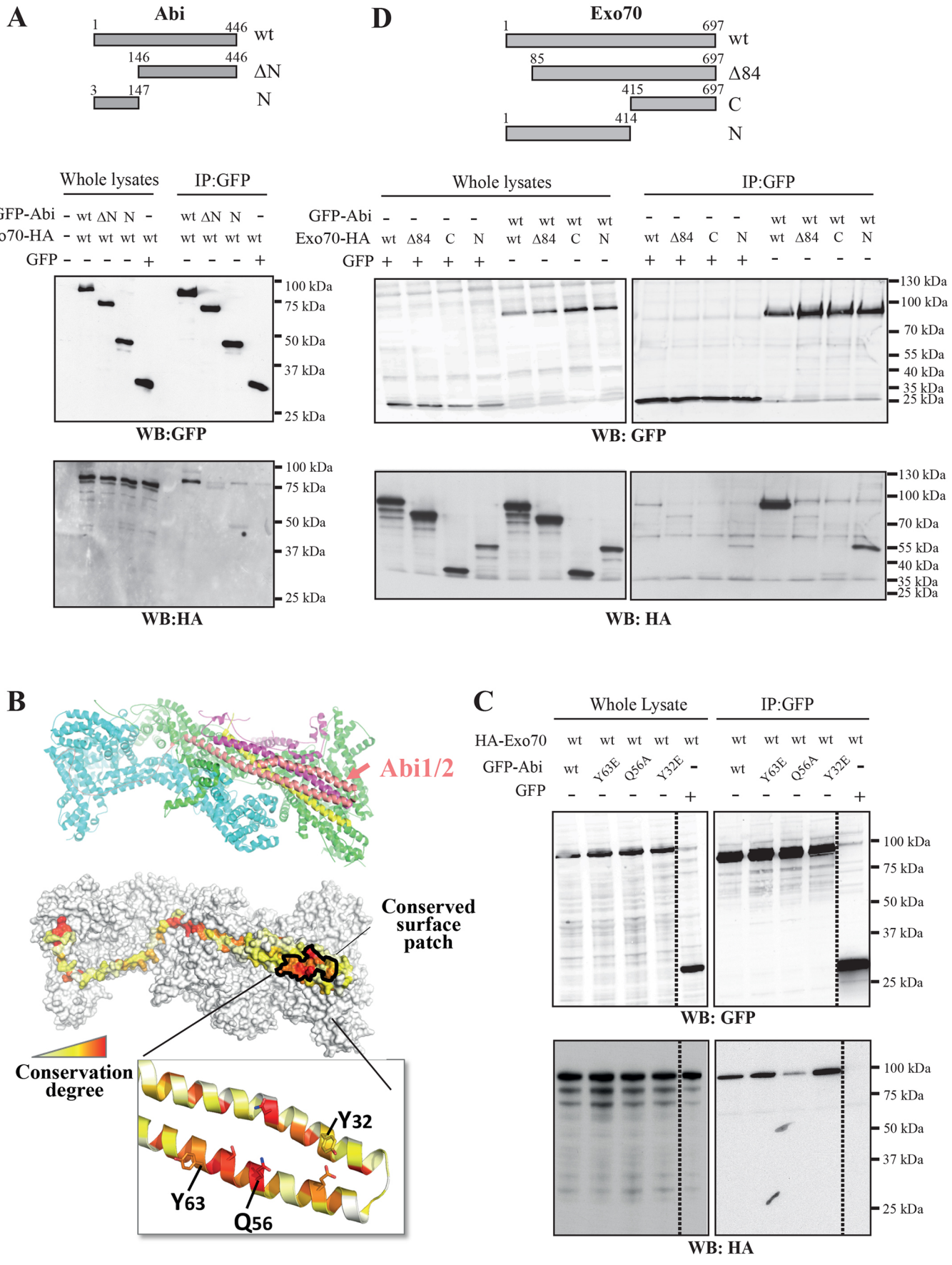

Fig. 4. See next page for legend.

Journal of Cell Science (2016) 129, 3756-3769 doi:10.1242/jcs.187336

Fig. 4. Mapping of the Exo70–Abi1 interaction surface. (A) The Abi–Exo70 interaction is mediated by the N-terminal domain of Abi proteins. HEK293 cells were transiently transfected, as indicated, with vectors expressing Exo70–HA and various GFP–Abi1 (GFP–Abi) constructs: Abi1, transcript variant 8, full-length (wt, residues 1–446), ΔN (residues 146–446); Abi2 N-terminal (N, residues 3–147). GFP fusions were immunoprecipitated and pulled-down proteins were analyzed by western blotting (WB) for GFP (upper panel) and HA (lower panel). Non-specific shadows of GFP fusions appear in the anti-HA blot owing to their large amount. (B) Structural localisation of Abi1 in the context of the WRC (noted as Abi1/2 given that Abi2, the close paralog of Abi1, is likely to bind in the same way). Top figure represents the various subunits of the WRC as cartoons (Protein Data Bank ID 3pc8) in different colors with Abi as light pink. The bottom figure is a surface representation of the WRC in which the surface of Abi1 has been colored with respect to the conservation of its residues [from white (divergent positions) to red (invariant ones)]. The insert is a zoomed image of the conserved surface patch and highlights three residues Y32, Q56 and Y63 of this patch as sticks, which are very exposed in the WRC and conserved. (C) The conserved Q56 residue of Abi1 mediates binding to Exo70. The experiment was performed as that described in A, comparing Abi1 wild type with three point mutants: Y63E, Q56A, Y32E. (D) The Abi1–Exo70 interaction is mediated by the first 84 N-terminal residues of Exo70. The experiment was performed as described in panel A with additional Exo70 constructs as indicated.

preferential directionality with respect to the cell front. We therefore divided the protrusions into three categories according to their status: nascent, active and ending (see Materials and Methods for technical definitions). This categorization clearly revealed that the nascent protrusions present a strong dominance of consistent anterograde flow of WRC (Fig. 6C; Fig. S2A and B).

In parallel, we attempted to apply a similar approach to cells expressing GFP–Sec6, with the aim of correlating WRC and exocyst translocation dynamics. Disappointingly, neither by correlation methods nor by particle tracking, we could not obtain any evidence of Sec6 directed flows, instead, we found a diffusion-like motion (Fig. S3A, B and C; Movie 3). These results indicate that exocyst trafficking, even if presumably polarized toward the front, remains very difficult to visualize, possibly because of the continuous fast recycling of this complex (Rivera-Molina and Toomre, 2013) or because the exogenous GFP–Sec6 cannot fully recapitulate the behavior of the endogenous Sec6.

In conclusion, by using this novel correlation-based image analysis approach, we could show that in nascent protrusions, the majority of WRC molecules travel toward the front edge, where they are subsequently recruited.

Correlation between WRC recruitment and edge velocity at protrusion sites

We quantified the dynamic recruitment of GFP–Abi1 at protrusive sites by precisely measuring in time (images every 2 s) and space (100× magnification) the intensity of the GFP fluorescence at the cell periphery. In parallel, we also measured the velocity of the edge movements. To do so, we implemented a freely available ImageJ plugin (see Materials and Methods). This plugin allows computation of the fluorescence intensity at the cell edge and the edge velocity, for each time point and for each position along the edge. An overview of the results is given by kymograph representations, as shown in Fig. 7A, for a representative cell region (Movie 2) – GFP–Abi1 (i.e. WRC) displays a dynamic spatio-temporal profile of recruitment at protrusion edges, which mirrors the spatio-temporal profile of edge velocity.

To mathematically confirm these observations, we computationally calculated the spatio-temporal correlation between WRC recruitment and edge velocities for several protrusive regions, following a previously reported method (Machacek et al., 2009). Notably, this analysis showed that the maximum correlation values were narrowly distributed around a time lag of 0 s (Fig. 7B). The computed averaged time delay between edge advancement and WRC recruitment (averaged time lag=−1.6 s±0.66 s, n=10 protrusions) was below our acquisition time interval (2 s). This finding indicates that WRC recruitment is synchronous with edge movement, at least within the limit of our temporal resolution. In other words, as soon as WRC is recruited, the edge moves forward and, as soon as WRC leaves, the edge stops moving or starts retracting. This striking spatio-temporal correlation underscores a possible cause–effect relationship between WRC translocation and protrusion.

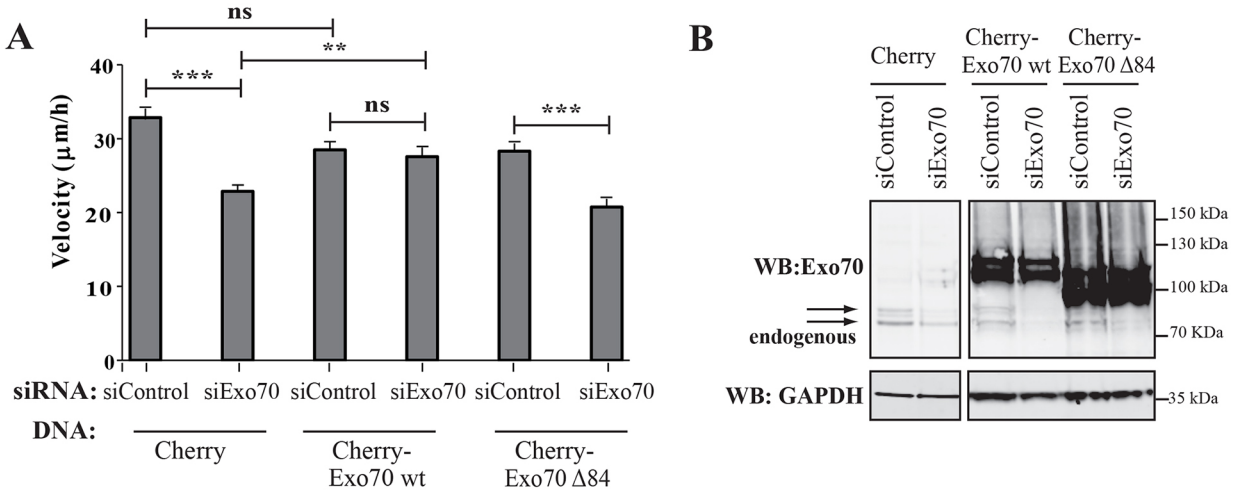

Fig. 5. Exocyst–WRC association contributes to cell migration. (A) Deletion of the first 84 N-terminal residues of Exo70 impairs cell migration. At day 0, HEK-HT cells were treated with an siRNA targeting an untranslated region in Exo70 mRNA (siExo70). At day 1, cells were transfected with vectors expressing Cherry alone, Cherry-fused Exo70 wild type (wt) or Exo70 Δ84 mutant. At day 3, Cherry-positive populations were sorted by using fluorescence-activated cell sorting (FACS) and plated at low density for random-motility assays. Time-lapse videos were acquired overnight and quantified by using ImageJ plugin Manual Tracking. n>50 cells from two independent experiments. The mean values were plotted. Error bars represent s.e.m. Asterisks indicate the results of one-way ANOVA test: **P<0.01; ***P<0.001; ns, not significant. (B) Validation of endogenous Exo70 depletion and exogenous Exo70 expression. Representative western blots (WB) of lysates prepared at day 3 from cells used in A. Arrows indicate the two predomiant endogenous Exo70 isoforms.

Journal of Cell Science (2016) 129, 3756-3769 doi:10.1242/jcs.187336

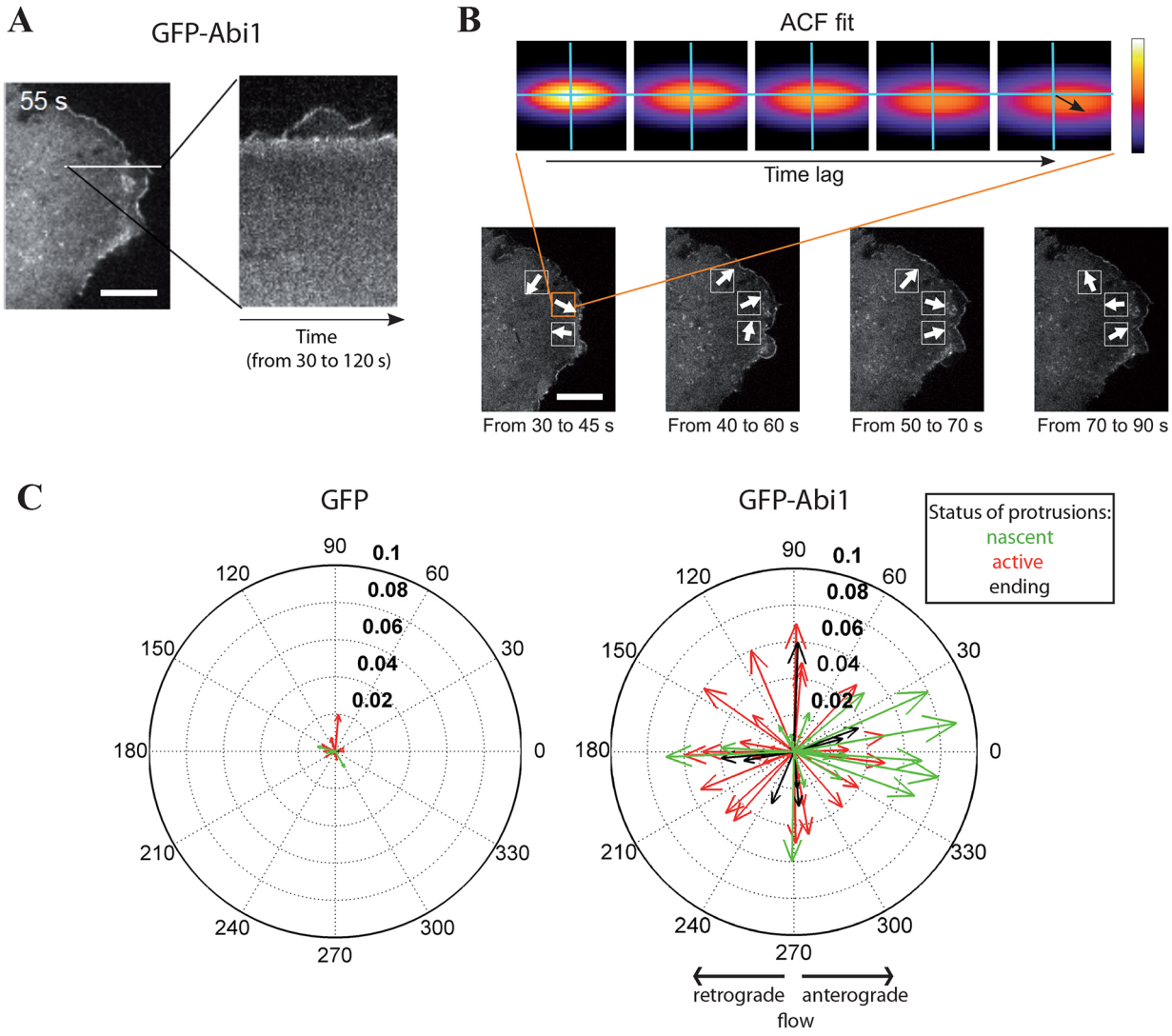

Fig. 6. Identification of a forward flow of WRC. (A) Visualization of WRC dynamics. A motile HEK-HT cell expressing GFP–Abi1 was imaged by confocal spinning-disc fast-acquisition imaging. See Movie 1 for the entire sequence. A kymograph was generated along the indicated line crossing the membrane. It shows the sharp recruitment of GFP–Abi1 at the edge of a nascent and expanding protrusion. Scale bar: 10 µm. (B) WRC molecular flow estimation by using local STICS analysis. Three regions of interest at the front of the representative cell shown in panel A were analyzed at four indicated time intervals by using the ImageJ plugin MICS Toolkit (see Materials and Methods). White arrows indicate the direction of detected Abi1 molecular flows. The upper part shows an example of Gaussian fitting of the spatial autocorrelation function (ACF) computed for increasing time lag (3-s lag between images) and the resultant peak displacement (black arrow in the last image), which indicates both the direction of flow and its magnitude. Scale bar: 10 µm. (C) Polar plots of flow vectors measured by using STICS for GFP–Abi1 and GFP alone. The protrusions were classified according to their status as nascent, active or ending (see Materials and Methods). The arrows represent flow measurements on eight cells for GFP–Abi1 (>6 measurements per cell, for a total of 82 measurements) and three cells for GFP (>5 measurements per cell, for a total of 20 measurements). The color of the arrow indicates the status of the analyzed protrusion: nascent (green), active (red), ending (black). The length of the arrows represents the flow velocity (µm/s), whereas the angle of the arrows represents the flow direction (the angle is measured between the direction of the flow vector and the perpendicular to the tangent of the cell borders; angle=0° corresponds to a perfectly anterograde flow). Essentially, no flow was detected in GFP cells, whereas several strong multidirectional flows in the order of 0.04–0.08 µm/s were measured in GFP–Abi1 cells (see also speed distribution in Fig. S2A). Most of the GFP–Abi1 flows in the case of nascent protrusions were directed toward the front (see also angle distribution in Fig. S2B).

Exocyst is required for optimal WRC recruitment and edge velocity

We questioned the necessity of the Ral–exocyst pathway for optimal WRC recruitment by staining the endogenous Wave2 subunit of HEK-HT cells that had been fixed during random motility. The depletion of exocyst subunits (Sec6, Exo70 or Sec5), as well as of Ral proteins (RalA and RalB), reduced the fraction of the cell perimeter that was positive for Wave2, without substantially perturbing total cell perimeter (Fig. 8A; see Fig. S4A for validation of depletions). The expression of constitutively active Rac1V12 has been previously reported to increase WRC recruitment at the cell membrane periphery (Steffen et al., 2004), probably because of a retention effect after WRC translocation. We reproduced this finding by overexpressing RFP–Rac1V12 in our cell system (compare siControl in Fig. 8A versus B). In addition, we found that, also in Rac1V12-expressing cells, the depletion of exocyst subunits or of Ral proteins reduced the staining of Wave2 at the cell perimeter (Fig. 8B; Fig. S4A), indicating that both exocyst and active Rac1 are required for maximal WRC recruitment.

The observation that both RalA and RalB depletion affects WRC recruitment was surprising because RalB, but not RalA, has

Journal of Cell Science (2016) 129, 3756-3769 doi:10.1242/jcs.187336

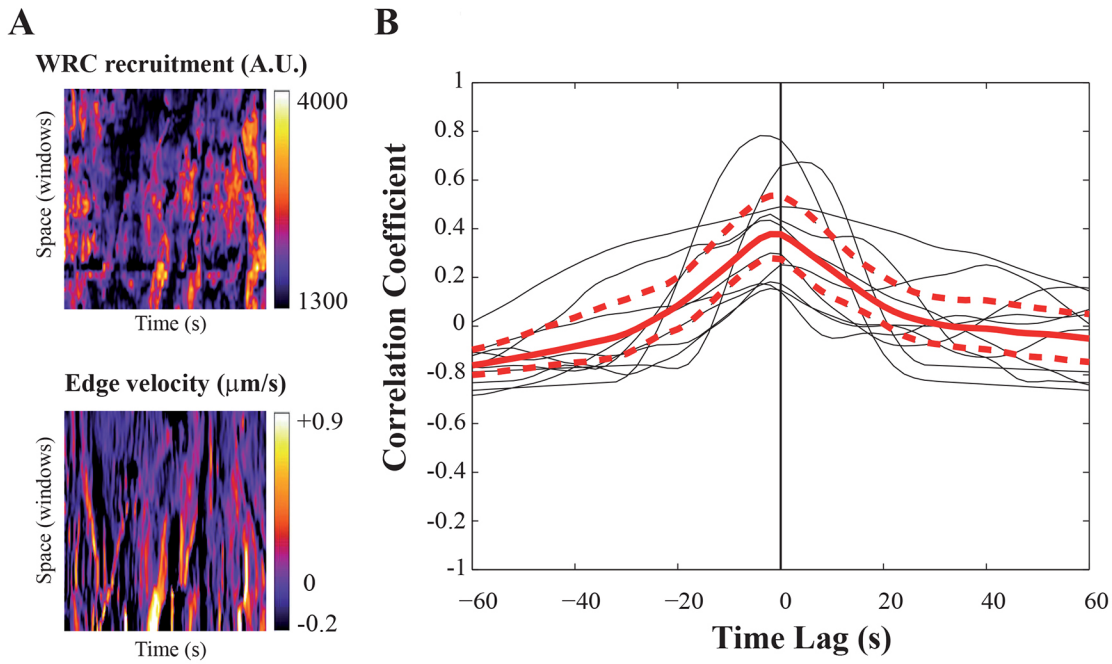

Fig. 7. Synchronicity between WRC recruitment and edge velocity. (A) Dynamics of WRC recruitment and cell edge movements. The homemade ImageJ plugin Recruitment Edge Dynamics (see Materials and Methods) was used to analyze a representative protrusion. See Movie 2 for the entire sequences. The obtained kymographs show the spatio-temporal dynamics of WRC recruitment and edge velocity. The apparent correlation between these two measurements can be seen even by eye: high WRC-recruitment values correspond to positive edge velocities (i.e. protrusion), whereas low WRC fluorescence at the edge corresponds to close-to-0 or negative edge velocities (i.e. static edge or retraction). (B) Temporal cross-correlation between WRC recruitment and edge velocity. Each black line represents an individual protrusion. Maximum correlation values were narrowly distributed around time lags of 0 s, indicating that WRC recruitment is synchronous with edge movement. The red line represents the average temporal cross-correlation function (n=10 protrusions from 6 cells).

been reported to be necessary for motility in various cell models (Lim et al., 2006; Oxford et al., 2005; Rossé et al., 2006). When we assessed the effect of Ral silencing on the motility of HEK-HT cells, we observed an inhibition upon RalA depletion, which was milder than that upon RalB depletion (Fig. S4B). This suggests that RalA could, indeed, have a role in cell motility in HEK-HT cells.

In addition, we performed experiments in live cells using Cherry–Abi1 as a quantifiable sensor of WRC recruitment. In selected front regions, as in Fig. 7A, we computed Cherry–Abi1 fluorescence at the cell edge, and we measured the fluctuation of WRC recruitment by calculating the coefficient of variation of Cherry–Abi1 fluorescence over the time and over the edge length. In cells depleted of Sec6 or Exo70, there was a significant decrease in the fluctuation of WRC recruitment with respect to control cells (Fig. 8C; Movie 4), indicating that exocyst is necessary for the normal dynamics of WRC localization at leading edges. Consistent with the correlation described above between WRC recruitment and edge velocity, this defect of WRC recruitment dynamics was associated with a defect in edge velocity – the edges of Sec6- or Exo70-depleted cells protruded and retracted more slowly than control cells (Fig. 8D; Movie 4). Interestingly, both positive (protrusions) and negative velocities (retractions) were decreased in exocyst-depleted cells, suggesting that back and forward edge movements are intimately connected. Finally, as expected (Rossé et al., 2006), silencing of exocyst subunits inhibited cell velocity in a wound healing assay (Fig. S4B).

These results together strongly support the notion that exocyst promotes WRC recruitment at the leading edge, which in turn causes edge advancement, initiating a protrusion event and stimulating cell motility.

DISCUSSION

In this work, we show the existence of a physical association between exocyst, an important complex in exocytosis, and WRC, a crucial module in actin polymerization machinery, and we provide evidence for a functional role of this association in the recruitment of WRC to specific plasma membrane sites where protrusions are formed in migrating cells.

How is WRC transported to the cell periphery and recruited to the leading edge of lamellipodia? This is a very crucial question in order to understand cell motility. Kinesin-mediated transport along microtubules has been proposed to bring WRC to the cell periphery in motile cells (Takahashi and Suzuki, 2008, 2009). Very interestingly, the exocyst has also been proposed to use microtubules tracks to target secretory vesicles. Exocyst has been shown to associate and colocalize with microtubules (Vega and Hsu, 2001; Xu et al., 2005). In neuronal cells, this association promotes neurite outgrowth (Vega and Hsu, 2001). Therefore, both WRC and exocyst might exploit microtubules for the long-distance travel to protrusions. Our work suggests that the direct interaction between WRC and exocyst might play a role in the short-distance travel of WRC inside the protrusions, resulting in its recruitment to the leading edge.

Other non-exclusive molecular mechanisms have been proposed for the role of exocyst in protrusion initiation and motility. In particular, two properties of Exo70 link this exocyst subunit to the migration machinery. Firstly, Exo70 directly binds to and stimulates the actin-nucleating Arp2/3 complex (Liu et al., 2012; Zuo et al., 2006); however, N-terminal truncation of Exo70 impairs cell migration despite the fact that Arp2/3 binding and stimulation are normal (Zhao et al., 2013), indicating that Exo70 can regulate cell migration also by a mechanism independent of direct Arp2/3

Journal of Cell Science (2016) 129, 3756-3769 doi:10.1242/jcs.187336

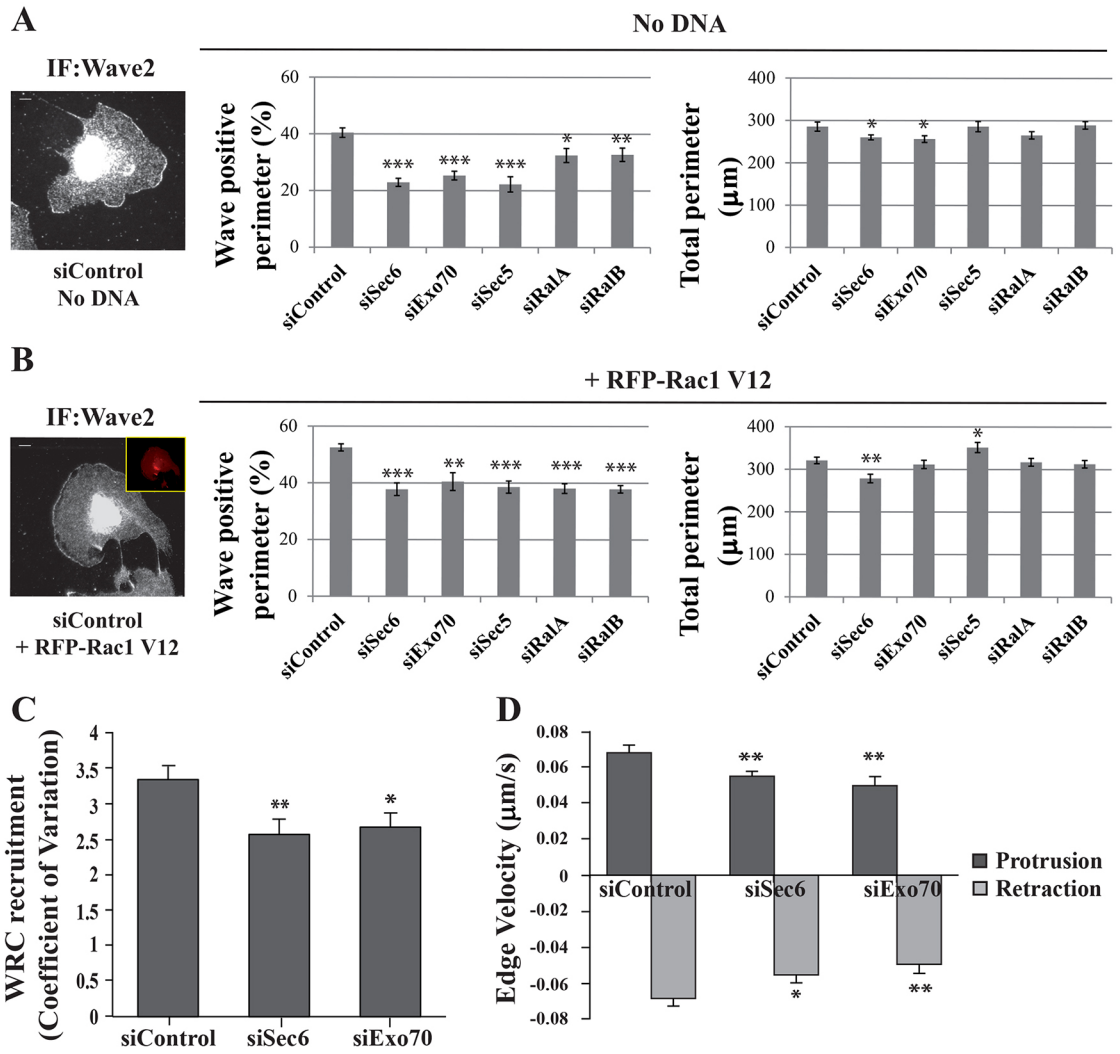

Fig. 8. Exocyst is required for optimal WRC recruitment and cell edge velocity. (A) Depletion of exocyst subunits, RalA or RalB, impairs Wave2 recruitment to protrusion edges. HEK-HT cells were transfected with siRNA against luciferase (siControl), Sec6 (siSec6), Exo70 (siExo70), Sec5 (siSec5), RalA (siRalA) or Ralb (siRalB). Three days later, randomly moving cells were fixed and immunostained for Wave2. Total cell perimeters and the fractions of cell perimeters positive for Wave2 were measured. The mean values (n>30 cells) were plotted. Representative cells are shown on the left. Scale bar: 10 µm. Error bars represent s.e.m. Asterisks indicate the results of Student's t-test analysis: *P<0.05, **P<0.01, ***P<0.001. (B) In RacV12-expressing cells, depletion of exocyst subunits, RalA or RalB, impairs Wave2 recruitment to protrusion edges. HEK-HT cells were co-transfected with the indicated siRNAs and with plasmid expressing RFP–RacV12. Red-fluorescent cells, expressing RacV12, were selected for analysis. Quantifications were performed as described in A. (C) Depletion of Sec6 or Exo70 impairs the dynamics of WRC recruitment. HEK-HT cells stably expressing Cherry–Abi1 were transfected with the indicated siRNAs. Kymographs of WRC recruitment dynamics were obtained as described in Fig. 7A (n>13 protrusions from n>9 cells per condition). We calculated for each protrusion the coefficient of variation, a statistical parameter defined as the ratio of the s.d. to the mean, and we expressed it as a percentage: (s.d./mean)×100. The coefficient of variation shows the extent of variability in relation to the mean of the population. Error bars represent Standard Error of the Mean (s.e.m.). Asterisks indicate the results of Student's t-test: *P<0.05, **P<0.01. (D) Depletion of Sec6 or Exo70 impairs cell edge velocity. Kymographs of cell edge speed were obtained as described in Fig. 5A (n>13 protrusions from n>9 cells per condition). Error bars represent s.e.m. Asterisks indicate the results of Student's t-test: *P<0.05, **P<0.01.

stimulation. Secondly, Exo70 can generate membrane curvatures *in vitro* and *in vivo* through an oligomerization-based mechanism. This Exo70 function does require the Exo70 N-terminal region (Zhao et al., 2013). Therefore, the Exo70 N-terminal coiled-coil region can mediate Exo70–Abi1 interaction, promoting exocyst–WRC association, as well as Exo70–Exo70 interactions, generating membrane curvature.

The X-ray structure of the whole exocyst complex has not been solved yet. However, the observation that multiple exocyst subunits can bind to the same partner is informative – Sec5 and Exo84 to Ral proteins (Moskalenko et al., 2003), Exo70 and Sec6 to WRC (this work), Exo84 and Sec8 to SH3BP1 (Parrini et al., 2011), Exo84 and Sec3 to WASH (Monteiro et al., 2013). This suggests that the exocyst subunits are intricately packed together, exposing composite surfaces for interaction with partners, as supported by the elongated exocyst architecture recently observed by using negative-stain electron microscopy (Heider et al., 2016).

We showed that the N-terminal coiled-coil motif of Exo70 (residues 1–84) and the N-terminal of Abi proteins (residues 1–146) are required for the Exo70–Abi interaction. Noteworthy, in the WRC, the N-terminal region of Abi2 was found to fold as a heteromeric coiled-coil structure with Brick1 and Wave1 (Chen et al., 2010). Interestingly, in the context of SNARE complexes, Abi1 has been reported to bind to syntaxin-1 and SNAP-25 through

a region spanning N-terminal residues 54–108 (Echarri et al., 2004). The latter two proteins are known to interact with their partners through coiled-coil bundles (Sutton et al., 1998). Altogether, these elements suggest that the N-terminal regions of Abi1 and Abi2 are prone to form triple helix coiled-coils with a versatile set of binding partners, and point to a possible similar mechanism for the interaction with Exo70. The roles of Exo70 dimerization, its incorporation into the exocyst complex and its interaction with the WRC remain to be clarified.

MATERIALS AND METHODS

Yeast two-hybrid methods

The coding sequence for full-length human EXOC7 variant 1 (homolog of *S. cerevisiae* Exo70) (GenBank accession: NM_001013839) was cloned into pLex12 as a C-terminal fusion to LexA. The coding sequence for residues 297–745 of human EXOC3 (homolog of *S. cerevisiae* Sec6) (GenBank accession: NM_007277) was cloned into pB27 as a C-terminal fusion to LexA. The constructs were used as a bait to screen at saturation a highly complex randomly primed human placenta cDNA library constructed into pP6. About 100 million clones (seven times the complexity of the library) were screened using a mating approach with Y187 (matα) and L40ΔGal4 (mata) yeast strains, as previously described (Formstecher et al., 2005; Fromont-Racine et al., 1997). 380 colonies in the Exo70 screen and 190 colonies in the Sec6 screen were selected on a medium lacking tryptophan, leucine and histidine. The prey fragments of the positive clones were amplified with PCR, sequenced at their 5′ and 3′ junctions and identified in GenBank (NCBI).

Cell culture, transfections, plasmids and siRNAs

Cells were grown in Dulbecco's modified Eagle's medium supplemented with 2 mM glutamine, penicillin, streptomycin, 10% fetal bovine serum. See Table S1 for detailed information and selection antibiotics. All cell lines were routinely verified to be free of mycoplasma by using a PCR detection method (Venor®GeM Classic, Minerva Biolabs).

Transient DNA transfections were performed with Lipofectamine Plus reagents (Invitrogen) or JetPRIME (Polyplus). Transient double siRNA and DNA transfections were performed with RNAiMAX (Invitrogen) and JetPEI (Polyplus). See Tables S2 and S3 for plasmid and siRNA sequences used in this work.

In vitro interaction assays

GST–Sec6 and GST–Exo70 were produced in Rosetta2 or BL21 *E. coli* strains by addition of 0.5 mM IPTG at 20–25°C for 4 h. Only a fraction of the expressed GST fusion was soluble, leading to poor yields (about 50 µg per 1 liter of culture). Abi1, the bi-molecular Nap1–Cyfip1 complex and the whole pentameric WRC were purified as previously reported (Innocenti, 2004; Derivery et al., 2009). The active Rac1 protein (Q61L mutant) was purified from *E. coli* (Self and Hall, 1995).

For the interaction assays shown in Fig. 1C,D and Fig. 1B, protein-loaded beads and purified proteins were incubated for 2 h at 4°C in a 300-µl final volume of interaction buffer A (50 mM Tris-HCl pH 7.5, 150 mM NaCl, 1% Triton X-100, 5% glycerol, freshly supplemented with protease inhibitor cocktail and 1 mM DTT). The amount of the input soluble proteins (Abi1, GST–Sec6, GST–Exo70) was 10–30 µg.

The competition assay in Fig. 1E was performed for 2 h at 4°C in a 300-µl final volume of interaction buffer B (20 mM Tris-HCl pH 8, 150 mM NaCl, 10% glycerol, 5 mM $MgCl_2$, freshly supplemented with protease inhibitor cocktail and 1 mM DTT).

Immunoprecipitations

For the immunoprecipitations, protein lysates from two 15-cm dishes were prepared in 1 ml per dish of lysis buffer C (50 mM Hepes, 150 mM NaCl, 1% NP-40, 0.1% sodium dodecyl sulfate, 0.5% sodium deoxycholate, 5 mM EDTA, pH 7.7, freshly supplemented with protease inhibitor cocktail and 1 mM DTT). For immunoprecipitation of Flag, lysates were incubated for 2 h at 4°C with 25 µl of agarose beads or magnetic beads coupled to FlagM2 antibody (Sigma-Aldrich), then washed five times with 1 ml of lysis buffer C and finally boiled in gel-loading buffer. For immunoprecipitation of V5, lysates were incubated (i) for 2 h at 4°C with 7 µl of agarose beads coupled to anti-V5 antibody (Sigma-Aldrich) or (ii) for 1 h at 4°C with 10 µg of anti-V5 antibody (Invitrogen), followed by 1 h at 4°C with 20 µl of magnetic beads coupled to G protein (Invitrogen). Beads were washed three times with high-salt buffer (lysis buffer with 500 mM NaCl) and three times in low-salt buffer (lysis buffer lacking NaCl).

For immunoprecipitation with overexpressed proteins (Fig. 4), lysates from one 6-cm dish were prepared in 0.6 ml lysis buffer D (50 mM Tris-HCl pH 7.5, 150 mM NaCl, 1% Triton X-100, 1 mM EDTA, freshly supplemented with protease inhibitor cocktail and 1 mM DTT). Lysates were incubated for 1 h at 4°C with magnetic beads coupled to anti-GFP antibody (ChromoTek). Beads were washed three times with the same buffer.

Immunofluorescence staining

Cells were fixed with 4% paraformaldehyde for 15 min and permeabilized for 5 min with 0.1% Triton X-100 or 0.5% NP40. See Table S4 for antibodies. In order to quantify the recruitment of Wave2 at the cell edges of random motile cells (Fig. 6A and B), for each cell, we manually draw and measured, by using ImageJ software, the total cell perimeter (a) and the perimeter portion positive for Wave2 staining (b). The 'Wave-positive perimeter' percentage was calculated as (b/a)×100.

Western blots

See Table S4 for antibodies. Detection was achieved with the ECL chemiluminescence method (PerkinElmer, #NEL104001EA) using horseradish peroxidase (HRP)-conjugated secondary antibodies (Jackson ImmunoResearch) or with the LICOR Odyssey Infrared Imaging System (LI-COR Biosciences) using IRDye-conjugated secondary antibodies.

Fast-acquisition spinning-disc microscopy

Cells were imaged on a Nikon Ti inverted microscope equipped with an EMCCD camera, a spinning disc (Yokogawa CSU-X1) with four-laser line, a heated chamber and CO_2 controller (Life Imaging Services), under control of the MetaMorph software (Universal Imaging). Images were acquired every 1 or 2 s, using a 100× NA1.4 oil immersion objective.

Spatio-temporal image correlation spectroscopy

Protrusions were searched for visually in the spinning-disc movies. STICS measurements were performed on a region of interest (ROI) of 32×32 pixels (5.12×5.12 µm), with a ROI center at about 3–5 µm and a ROI edge at ∼1–2 µm from the closest cell edge, in order to avoid a border effect. If obvious vesicles were visible in the ROI, the measurements were discarded. We developed and used the plugin MICS Toolkit (downloaded from http://minilien.curie.fr/dr8ep8), based on previous work (Brown et al., 2006; Kolin and Wiseman, 2007). First, image correlation spectroscopy (ICS) was performed on a set of three images in order to check for the point spread function (PSF) of the experiment. Then, STICS analysis was performed on the selected ROI on time windows of 20 frames (20–40 s depending on the microscope acquisition setting). Gaussian fitting of the spatiotemporal correlation function was visually checked, and only the lag times for which it appeared correct were considered for the linear fitting of the displacement of the peak. The ROI was considered as having a flow only if the displacement of the peak against lag times was monotonic in both x and y. An average velocity for the selected time period and a direction were then obtained. The velocity values were coherent with temporal image correlation spectroscopy (TICS) measurements of a population undergoing both diffusion and flow. We used homemade *in silico* simulations, using parameters (density, diffusion, flow) similar to those observed in cells, to validate the robustness of the method (not shown).

A time widow of a specific ROI was classified as 'nascent protrusion' when the last two to three frames (out of 20) showed the front edge starting to move forward. It was classified as an 'active protrusion' when the front edge was actively moving during the entire sequence. It was classified as

'ending protrusion' when retraction was clearly observed during the temporal sequence. When possible, the same ROI was analyzed in the various protrusion states.

Cell-edge tracking, recruitment measurement and cross-correlation analysis

Cells were cropped around the protrusions. The edge segmentation over time was achieved by creating and using an ImageJ threshold function, and a time-lapse binary mask, which was visually checked and manually corrected when needed. Starting from the original image and from the binary mask, we then used a custom-made ImageJ plugin, named Recruitment Edge Dynamics (which can be downloaded from http://minilien.curie.fr/pnj9m7), which tracks, over the time, uniformly sampled points (windows) to generate two maps. The first map represents the protein recruitment – i.e. the maximum fluorescent intensity at the edge (width of 0.8 µm) for each window (in y) and for each timeframe processed (in x). The second map represents the speed of the edge for the same times and windows; positive speed indicates a protrusion, speed equal to zero indicates a static edge, whereas negative speed indicates a retraction. For cell-edge tracking, an approximate center of gravity of the cell was manually defined (outside of the image because cells had been cropped); a line passing by this center of gravity and by the sampled point at t was used to define the point position at t+1 as its intersection with the edge at t+1.

To compute the temporal cross correlation between protein recruitment and edge speed, we used a custom-made MATLAB program [which can be downloaded from http://xfer.curie.fr/get/Zn3LkZP0wDG/Correlation.zip, for Windows 64bits only, need MRC installer version 8.1 (2013 A) available freely from the MathWorks website, source code at http://xfer.curie.fr/get/Zn3LkZP0wDG/Correlation.zip]. Similar to the method of Machacek et al. (2009), we averaged by spline fitting the correlation of edge speed and recruitment over time for each protrusion, and we considered the correlation as significant if it passed the two following criteria: (1) the averaged maximum value of the cross-correlation coefficient was superior to the 90% confidence level of the correlation coefficient, depending on the number of sampled points; (2) the confidence interval of the spline fitting, computed by bootstrapping 2000 samples from the residuals, did not include 0. Correlation curves for individual protrusions were then merged to obtain the averaged maximum of correlation, corresponding to the time lag, and to calculate a confidence interval for this value.

Acknowledgements

We greatly thank the staff of the PICT-IBiSA imaging facility for their excellent assistance, Hybrigenics staff for yeast two-hybrid analysis and Nathalie Brandon for technical help. Some experiments were performed on the PICT-IBiSA (Institut Curie, Paris), member of the French National Research Infrastructure France-BioImaging (ANR-10-INSB-04).

Competing interests

The authors declare no competing or financial interests.

Author contributions

M.B., A.S.-D., G.Z., M.A., M.C.P. performed the biological experiments. P.P.-G., F.W., M.C.P. developed image analysis codes and analyzed the data. E.F. coordinated 2-hybrid screens. M.H., A.G. generated cell lines. J.Y., R.G. performed structural modeling. M.C.P., G.S., J.C., A.G. designed and supervised the experiments. M.C.P. wrote the manuscript. A.S.-D., P.P.-G. and G.Z. made equal contributions to this work, as did G.S., J.C. and M.C.P.

Funding

This work was supported by Association pour la Recherche sur le Cancer [grant numbers SFI20121205710 to M.C.P. and SFI20111203931 to J.C.]; Ligue Contre le Cancer [grant number RS14/75-54 to M.C.P.]; Association Christelle Bouillot (to J.C.); GenHomme Network [grant number 02490-6088, to Hybrigenics and Institut Curie); Associazione Italiana per la Ricerca sul Cancro [grant number IG 14104 to G.S.); the European Research Council [grant number 268836 to G.S.]; the Association for International Cancer Research [grant number 14-0335 to G.S.]; and the Fondazione Cariplo (to G.S.). M.B. and A.S.-D. were recipients of fellowships from Association pour la Recherche sur le Cancer, Ligue Contre le Cancer, European Molecular Biology Organization and Vinci program of the Université Franco-Italienne.

Supplementary information

Supplementary information available online at
http://jcs.biologists.org/lookup/doi/10.1242/jcs.187336.supplemental

References

Abella, J. V. G., Galloni, C., Pernier, J., Barry, D. J., Kjær, S., Carlier, M.-F. and Way, M. (2016). Isoform diversity in the Arp2/3 complex determines actin filament dynamics. *Nat. Cell Biol.* **18**, 76-86.

Anitei, M., Stange, C., Parshina, I., Baust, T., Schenck, A., Raposo, G., Kirchhausen, T. and Hoflack, B. (2010). Protein complexes containing CYFIP/Sra/PIR121 coordinate Arf1 and Rac1 signalling during clathrin-AP-1-coated carrier biogenesis at the TGN. *Nat. Cell Biol.* **12**, 330-340.

Biondini, M., Duclos, G., Meyer-Schaller, N., Silberzan, P., Camonis, J. and Parrini, M. C. (2015). RalB regulates contractility-driven cancer dissemination upon TGFβ stimulation via the RhoGEF GEF-H1. *Sci. Rep.* **5**, 11759.

Brown, C. M., Hebert, B., Kolin, D. L., Zareno, J., Whitmore, L., Horwitz, A. R. and Wiseman, P. W. (2006). Probing the integrin-actin linkage using high-resolution protein velocity mapping. *J. Cell Sci.* **119**, 5204-5214.

Chen, Z., Borek, D., Padrick, S. B., Gomez, T. S., Metlagel, Z., Ismail, A. M., Umetani, J., Billadeau, D. D., Otwinowski, Z. and Rosen, M. K. (2010). Structure and control of the actin regulatory WAVE complex. *Nature* **468**, 533-538.

Derivery, E. and Gautreau, A. (2010). Generation of branched actin networks: assembly and regulation of the N-WASP and WAVE molecular machines. *Bioessays* **32**, 119-131.

Derivery, E., Lombard, B., Loew, D. and Gautreau, A. (2009). The Wave complex is intrinsically inactive. *Cell Motil. Cytoskeleton* **66**, 777-790.

Disanza, A., Carlier, M.-F., Stradal, T. E. B., Didry, D., Frittoli, E., Confalonieri, S., Croce, A., Wehland, J., Di Fiore, P. P. and Scita, G. (2004). Eps8 controls actin-based motility by capping the barbed ends of actin filaments. *Nat. Cell Biol.* **6**, 1180-1188.

Echarri, A., Lai, M. J., Robinson, M. R. and Pendergast, A. M. (2004). Abl interactor 1 (Abi-1) wave-binding and SNARE domains regulate its nucleocytoplasmic shuttling, lamellipodium localization, and wave-1 levels. *Mol. Cell. Biol.* **24**, 4979-4993.

Eden, S., Rohatgi, R., Podtelejnikov, A. V., Mann, M. and Kirschner, M. W. (2002). Mechanism of regulation of WAVE1-induced actin nucleation by Rac1 and Nck. *Nature* **418**, 790-793.

Formstecher, E., Aresta, S., Collura, V., Hamburger, A., Meil, A., Trehin, A., Reverdy, C., Betin, V., Maire, S., Brun, C. et al. (2005). Protein interaction mapping: a Drosophila case study. *Genome Res.* **15**, 376-384.

Fromont-Racine, M., Rain, J.-C. and Legrain, P. (1997). Toward a functional analysis of the yeast genome through exhaustive two-hybrid screens. *Nat. Genet.* **16**, 277-282.

Gautreau, A., Ho, H.-y. H., Li, J., Steen, H., Gygi, S. P. and Kirschner, M. W. (2004). Purification and architecture of the ubiquitous Wave complex. *Proc. Natl. Acad. Sci. USA* **101**, 4379-4383.

Hahn, W. C., Counter, C. M., Lundberg, A. S., Beijersbergen, R. L., Brooks, M. W. and Weinberg, R. A. (1999). Creation of human tumour cells with defined genetic elements. *Nature* **400**, 464-468.

He, B. and Guo, W. (2009). The exocyst complex in polarized exocytosis. *Curr. Opin. Cell Biol.* **21**, 537-542.

Hebert, B., Costantino, S. and Wiseman, P. W. (2005). Spatiotemporal image correlation spectroscopy (STICS) theory, verification, and application to protein velocity mapping in living CHO cells. *Biophys. J.* **88**, 3601-3614.

Heider, M. R., Gu, M., Duffy, C. M., Mirza, A. M., Marcotte, L. L., Walls, A. C., Farrall, N., Hakhverdyan, Z., Field, M. C., Rout, M. P. et al. (2016). Subunit connectivity, assembly determinants and architecture of the yeast exocyst complex. *Nat. Struct. Mol. Biol.* **23**, 59-66.

Innocenti, M., Zucconi, A., Disanza, A., Frittoli, E., Areces, L. B., Steffen, A., Stradal, T. E. B., Di Fiore, P. P., Carlier, M.-F. and Scita, G. (2004). Abi1 is essential for the formation and activation of a WAVE2 signalling complex. *Nat. Cell Biol.* **6**, 319-327.

Ismail, A. M., Padrick, S. B., Chen, B., Umetani, J. and Rosen, M. K. (2009). The WAVE regulatory complex is inhibited. *Nat. Struct. Mol. Biol.* **16**, 561-563.

Kobayashi, K., Kuroda, S., Fukata, M., Nakamura, T., Nagase, T., Nomura, N., Matsuura, Y., Yoshida-Kubomura, N., Iwamatsu, A. and Kaibuchi, K. (1998). p140Sra-1 (specifically Rac1-associated protein) is a novel specific target for Rac1 small GTPase. *J. Biol. Chem.* **273**, 291-295.

Kolin, D. L. and Wiseman, P. W. (2007). Advances in image correlation spectroscopy: measuring number densities, aggregation states, and dynamics of fluorescently labeled macromolecules in cells. *Cell Biochem. Biophys.* **49**, 141-164.

Lebensohn, A. M. and Kirschner, M. W. (2009). Activation of the WAVE complex by coincident signals controls actin assembly. *Mol. Cell* **36**, 512-524.

Leng, Y., Zhang, J., Badour, K., Arpaia, E., Freeman, S., Cheung, P., Siu, M. and Siminovitch, K. (2005). Abelson-interactor-1 promotes WAVE2 membrane translocation and Abelson-mediated tyrosine phosphorylation required for WAVE2 activation. *Proc. Natl. Acad. Sci. USA* **102**, 1098-1103.

Lim, K.-H., O'Hayer, K., Adam, S. J., Kendall, S. D., Campbell, P. M., Der, C. J. and Counter, C. M. (2006). Divergent roles for RalA and RalB in malignant growth of human pancreatic carcinoma cells. *Curr. Biol.* **16**, 2385-2394.
Liu, J., Zhao, Y., Sun, Y., He, B., Yang, C., Svitkina, T., Goldman, Y. E. and Guo, W. (2012). Exo70 stimulates the Arp2/3 complex for lamellipodia formation and directional cell migration. *Curr. Biol.* **22**, 1510-1515.
Lu, H., Liu, J., Liu, S., Zeng, J., Ding, D., Carstens, R. P., Cong, Y., Xu, X. and Guo, W. (2013). Exo70 isoform switching upon epithelial-mesenchymal transition mediates cancer cell invasion. *Dev. Cell* **27**, 560-573.
Lupas, A., Van Dyke, M. and Stock, J. (1991). Predicting coiled coils from protein sequences. *Science* **252**, 1162-1164.
Machacek, M., Hodgson, L., Welch, C., Elliott, H., Pertz, O., Nalbant, P., Abell, A., Johnson, G. L., Hahn, K. M. and Danuser, G. (2009). Coordination of Rho GTPase activities during cell protrusion. *Nature* **461**, 99-103.
Mendoza, M. C., Er, E. E., Zhang, W., Ballif, B. A., Elliott, H. L., Danuser, G. and Blenis, J. (2011). ERK-MAPK drives lamellipodia protrusion by activating the WAVE2 regulatory complex. *Mol. Cell* **41**, 661-671.
Millius, A., Watanabe, N. and Weiner, O. D. (2012). Diffusion, capture and recycling of SCAR/WAVE and Arp2/3 complexes observed in cells by single-molecule imaging. *J. Cell Sci.* **125**, 1165-1176.
Monteiro, P., Rossé, C., Castro-Castro, A., Irondelle, M., Lagoutte, E., Paul-Gilloteaux, P., Desnos, C., Formstecher, E., Darchen, F., Perrais, D. et al. (2013). Endosomal WASH and exocyst complexes control exocytosis of MT1-MMP at invadopodia. *J. Cell Biol.* **203**, 1063-1079.
Moskalenko, S., Tong, C., Rosse, C., Mirey, G., Formstecher, E., Daviet, L., Camonis, J. and White, M. A. (2003). Ral GTPases regulate exocyst assembly through dual subunit interactions. *J. Biol. Chem.* **278**, 51743-51748.
Nozumi, M., Nakagawa, H., Miki, H., Takenawa, T. and Miyamoto, S. (2003). Differential localization of WAVE isoforms in filopodia and lamellipodia of the neuronal growth cone. *J. Cell Sci.* **116**, 239-246.
Oxford, G., Owens, C. R., Titus, B. J., Foreman, T. L., Herlevsen, M. C., Smith, S. C. and Theodorescu, D. (2005). RalA and RalB: antagonistic relatives in cancer cell migration. *Cancer Res.* **65**, 7111-7120.
Parrini, M. C., Sadou-Dubourgnoux, A., Aoki, K., Kunida, K., Biondini, M., Hatzoglou, A., Poullet, P., Formstecher, E., Yeaman, C., Matsuda, M. et al. (2011). SH3BP1, an exocyst-associated RhoGAP, inactivates Rac1 at the front to drive cell motility. *Mol. Cell* **42**, 650-661.
Pathak, R., Delorme-Walker, V. D., Howell, M. C., Anselmo, A. N., White, M. A., Bokoch, G. M. and DerMardirossian, C. (2012). The microtubule-associated Rho activating factor GEF-H1 interacts with exocyst complex to regulate vesicle traffic. *Dev. Cell* **23**, 397-411.
Pupko, T., Bell, R. E., Mayrose, I., Glaser, F. and Ben-Tal, N. (2002). Rate4Site: an algorithmic tool for the identification of functional regions in proteins by surface mapping of evolutionary determinants within their homologues. *Bioinformatics* **18** Suppl. 1, S71-S77.
Ridley, A. J., Schwartz, M. A., Burridge, K., Firtel, R. A., Ginsberg, M. H., Borisy, G., Parsons, J. T. and Horwitz, A. R. (2003). Cell migration: integrating signals from front to back. *Science* **302**, 1704-1709.
Rivera-Molina, F. and Toomre, D. (2013). Live-cell imaging of exocyst links its spatiotemporal dynamics to various stages of vesicle fusion. *J. Cell Biol.* **201**, 673-680.
Rossé, C., Hatzoglou, A., Parrini, M.-C., White, M. A., Chavrier, P. and Camonis, J. (2006). RalB mobilizes the exocyst to drive cell migration. *Mol. Cell. Biol.* **26**, 727-734.
Scita, G. and Di Fiore, P. P. (2010). The endocytic matrix. *Nature* **463**, 464-473.
Self, A. J. and Hall, A. (1995). Purification of recombinant Rho/Rac/G25K from Escherichia coli. *Methods Enzymol.* **256**, 3-10.
Steffen, A., Rottner, K., Ehinger, J., Innocenti, M., Scita, G., Wehland, J. and Stradal, T. E. B. (2004). Sra-1 and Nap1 link Rac to actin assembly driving lamellipodia formation. *EMBO J.* **23**, 749-759.
Stradal, T., Courtney, K. D., Rottner, K., Hahne, P., Small, J. V. and Pendergast, A. M. (2001). The Abl interactor proteins localize to sites of actin polymerization at the tips of lamellipodia and filopodia. *Curr. Biol.* **11**, 891-895.
Sutton, R. B., Fasshauer, D., Jahn, R. and Brunger, A. T. (1998). Crystal structure of a SNARE complex involved in synaptic exocytosis at 2.4 A resolution. *Nature* **395**, 347-353.
Takahashi, K. and Suzuki, K. (2008). Requirement of kinesin-mediated membrane transport of WAVE2 along microtubules for lamellipodia formation promoted by hepatocyte growth factor. *Exp. Cell Res.* **314**, 2313-2322.
Takahashi, K. and Suzuki, K. (2009). Membrane transport of WAVE2 and lamellipodia formation require Pak1 that mediates phosphorylation and recruitment of stathmin/Op18 to Pak1-WAVE2-kinesin complex. *Cell. Signal.* **21**, 695-703.
Vega, I. E. and Hsu, S. C. (2001). The exocyst complex associates with microtubules to mediate vesicle targeting and neurite outgrowth. *J. Neurosci.* **21**, 3839-3848.
Welf, E. S. and Haugh, J. M. (2011). Signaling pathways that control cell migration: models and analysis. *Wiley Interdiscip. Rev. Syst. Biol. Med.* **3**, 231-240.
Xu, K.-F., Shen, X., Li, H., Pacheco-Rodriguez, G., Moss, J. and Vaughan, M. (2005). Interaction of BIG2, a brefeldin A-inhibited guanine nucleotide-exchange protein, with exocyst protein Exo70. *Proc. Natl. Acad. Sci. USA* **102**, 2784-2789.
Zhao, Y., Liu, J., Yang, C., Capraro, B. R., Baumgart, T., Bradley, R. P., Ramakrishnan, N., Xu, X., Radhakrishnan, R., Svitkina, T. et al. (2013). Exo70 generates membrane curvature for morphogenesis and cell migration. *Dev. Cell* **26**, 266-278.
Zuo, X., Zhang, J., Zhang, Y., Hsu, S.-C., Zhou, D. and Guo, W. (2006). Exo70 interacts with the Arp2/3 complex and regulates cell migration. *Nat. Cell Biol.* **8**, 1383-1388.

SUPPLEMENTARY FIGURES

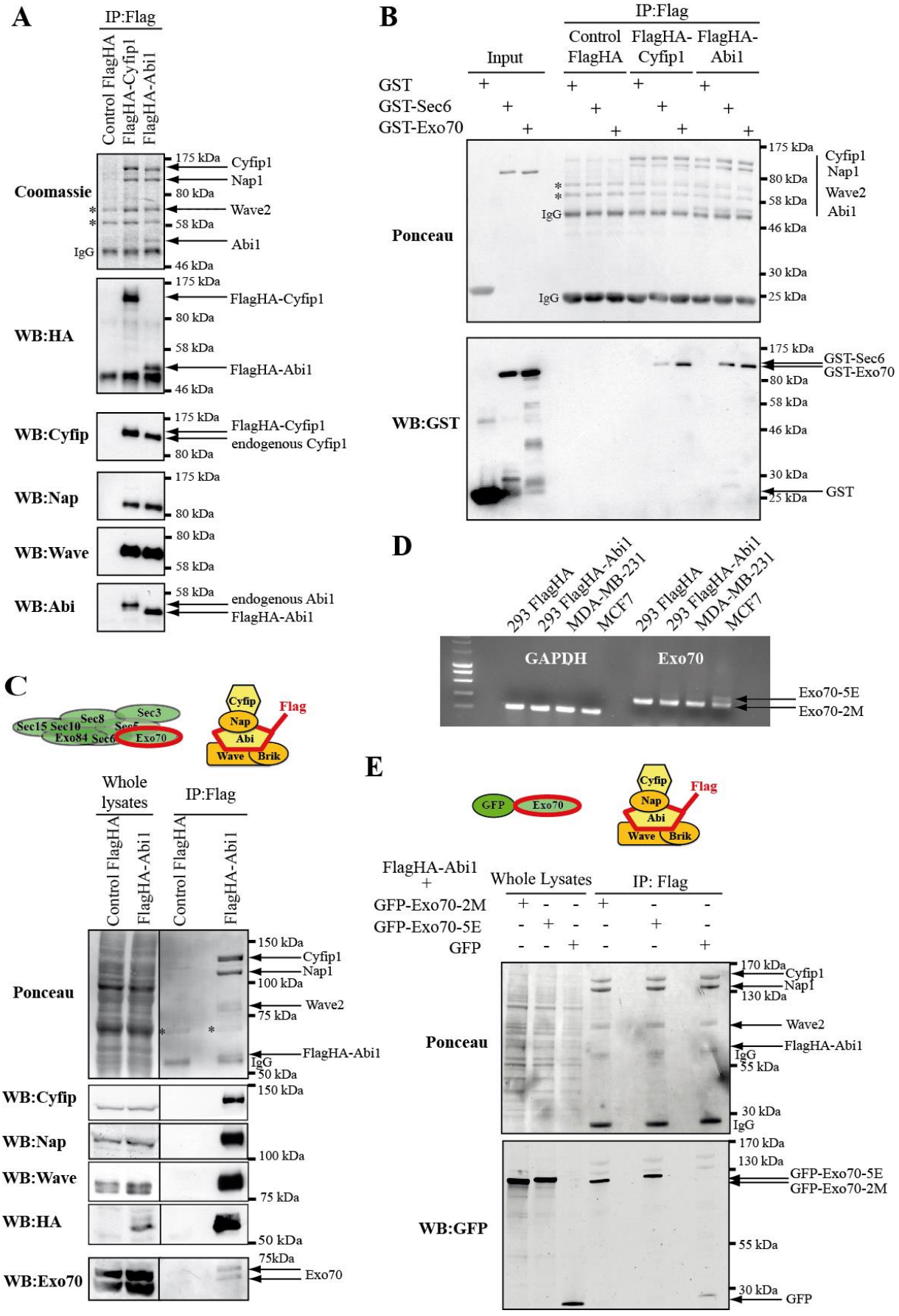

Supplementary Figure S1. Additional biochemical data.

(A-B) GST-Sec6 and GST-Exo70 directly interacts *in vitro* with the whole WRC complex. (A) The whole WAVE complex was purified from 293 human cells stably expressing Flag-HA-Cyfip1 or Flag-HA-Abi1 by immune-precipitation with anti-Flag antibodies. As negative control we performed anti-Flag IP from 293 cells expressing Flag-HA only. **(B)** The WAVE complex-coupled beads were incubated with GST alone, GST-Sec6 or GST-Exo70. After washing, pulled-down proteins were loaded on SDS-gel, transferred to membrane, stained with Red Ponceau and anti-GST antibodies

(C) WRC complex associates with endogenous Exo70. In 293 human cells stably expressing a Flag-HA-Abi1 construct, the whole WRC complex was immunoprecipitated with anti-Flag antibodies as shown by the Red Ponceau (upper panel) and the anti-Cyfip1, anti-Nap1, anti-Wave2, anti-Abi1 stainings (middle panel). A fraction of endogenous Exo70 co-precipitated with the WRC complex (lower panel). Note that in whole cell lysates two bands around 75 kDa are recognized by anti-Exo70 antibodies; both bands are specific, since both disappeared upon treatment with siRNA against Exo70 (Figures 5B and S4). * indicate non-specific bands.

(D) Expression of Exo70 isoforms in various cell lines, including our 293 cells expressing Flag-HA-Abi. The expression levels of Exo70 isoforms were analyzed by RT-PCR as reported (Lu et al., 2013). The primers used were:

AGGGCTGCTTTTAACTCTGGT and CCCCACTTGATTTTGGAGGGA (for GAPDH)

TGGCCGCAACCAAGATTTCATG and GAGAAGTCGTGTCGCACAATGGC (for Exo70)

(E) WRC complex associates with both Exo70-2M and Exo70-5E isoforms. Flag-HA-Abi1-expressing 293 cells were transfected with pEGFP plasmids expressing Exo70-2M, Exo70-5E (Lu et al., 2013) or GFP only as control. The WRC complex was immunoprecipitated with anti-Flag antibodies. Both Exo70 isoforms co-precipitated with the WRC complex.

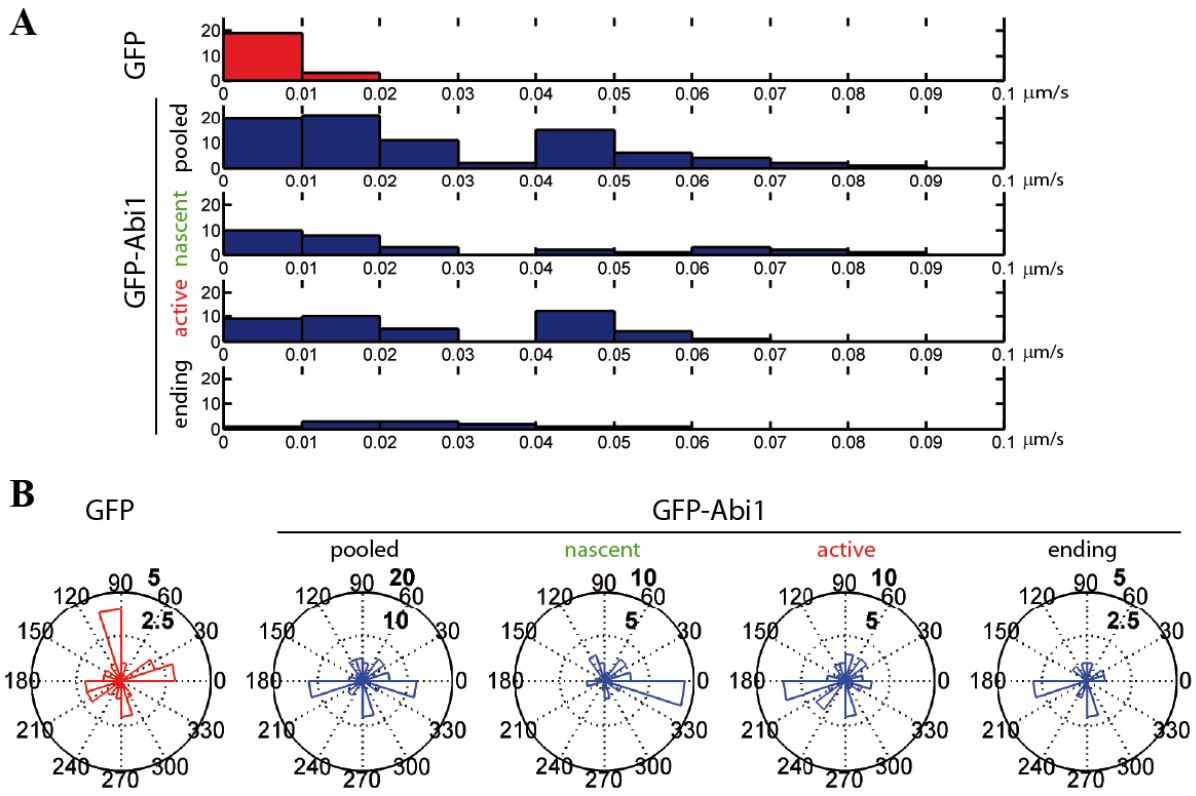

Supplementary Figure S2. Distribution of speeds and angles measured by STICS.

(A) Histograms of the speeds (flow norms). From top to bottom: pool of all measurements analyzed on GFP cells as control; pool of all measurements analyzed on GFP-Abi1 cells; and then for GFP-Abi1 cells, the three categories corresponding to nascent protrusions, active protrusions and ending protrusions. The distribution of GFP-Abi1 flow norms is not unimodal. There is one population with low (maybe inexistent) flow, and one around 0.05 µm/s. The fastest flows, up to 0.09 µm/s, are measured for nascent protrusions.

(B) Polar plots of the angle distribution. The angle is measured between the direction of the flow vector and the perpendicular to the tangent of the cell borders. Bold numbers indicates the scale of circles in number of regions analyzed. From left to right: pool of all measurements analyzed on GFP cells as control; pool of all measurements analyzed on GFP-Abi1 cells; and then for GFP-Abi1 cells, the three categories corresponding to nascent protrusions, active protrusions and ending protrusions. The distribution of GFP-Abi1 flow angles is multimodal. In particular, a majority of region of interest shows an anterograde flow for nascent protrusions, and a retrograde flow for active and ending protrusions.

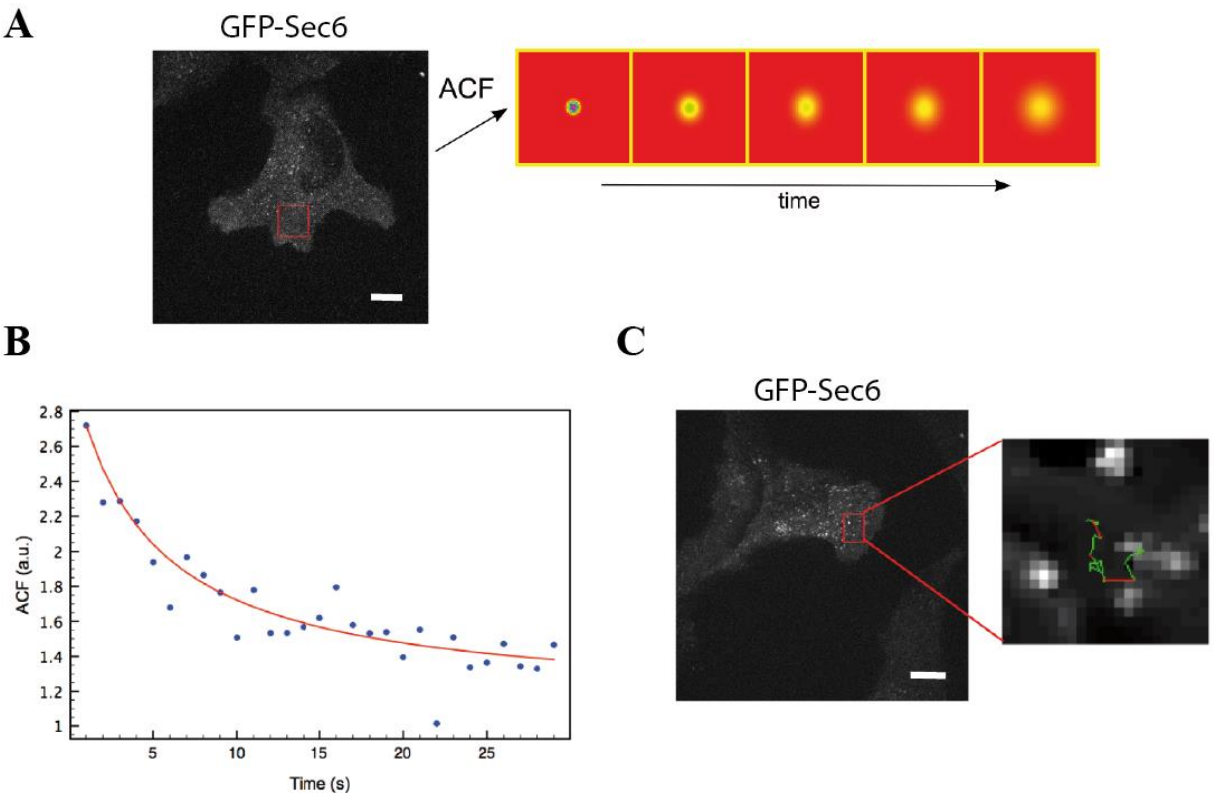

Supplementary Figure S3. GFP-Sec6 shows a random motion by several imaging analysis methods.

HEK-HT cells stably expressing GFP-Sec6 were generated using retroviruses.

(A) Representative STICS analysis. The indicated region of a HEK-HT cell expressing GFP-Sec6 was analyzed by STICS. The autocorrelation function (ACF) stays centered (no flow) but widens over time, which is a signature of diffusive type of motion. Scale bar, 10 μm.

(B) Time autocorrelation (TICS) analysis. The points fit well when using a diffusion model (red curve).

(C) Particle tracking. Fluorescent dots in the indicated region of a HEK-HT cell expressing GFP-Sec6 were analyzed by particle tracking. The zoomed image shows an example of a random-motion trajectory on an image subsequence after denoising by ND-Safir software. Scale bar, 10 μm.

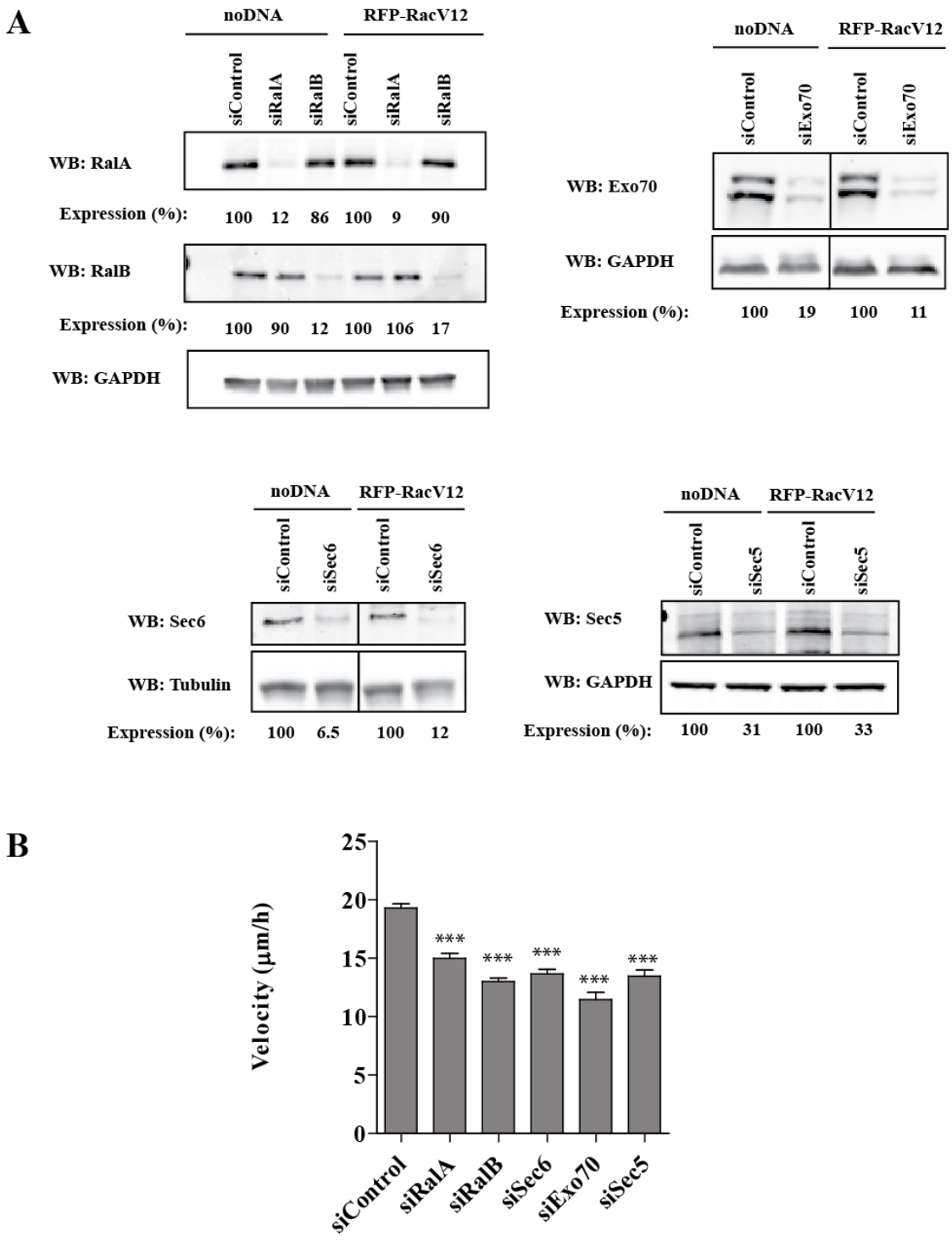

Supplementary Figure S4.

(A) Validation of protein depletions. HEK-HT were transfected with siRNAs (siControl, siRalA, siRalB, siExo70, siSec6 or siSec5), and with plasmid expressing RFP-RacV12 when indicated. Lysates were analyzed with the indicated antibodies. Protein expression levels, after normalization of protein loads using GAPDH or tubulin, are expressed as percentage of the controls.

(B) Depletion of RalA, RalB and Exocyst subunits inhibits motility of HEK-HT cells. Cells were depleted of indicated proteins, subjected to wound-healing assay and manually tracked as previously described (Parrini et al., 2011). n>62 cells per condition, from at least 3 independent experiments. Error bars represent Standard Error of the Mean (SEM). Asterisks indicate the results of Student t-test: *** <0.001.

SUPPLEMENTARY MOVIES

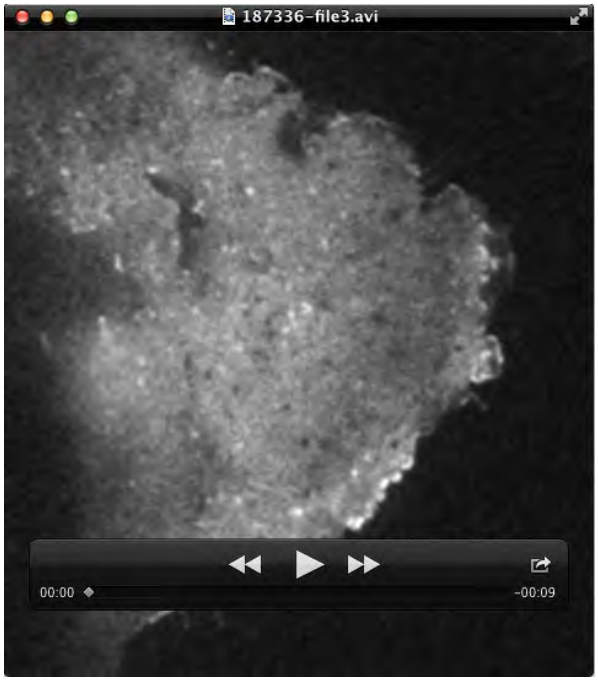

Movie 1. WRC dynamics in a motile cell. A HEK-HT cell, expressing GFP-Abi1, was visualized for 5 min (1 frame/s) by confocal spinning-disk microscopy.

Movie 2. WRC recruitment at the front. A front region from the cell of Movie S1 was selected and analyzed by the plugin Recruitment Edge Dynamics. The resulting kymographs are shown in Figure 5A.

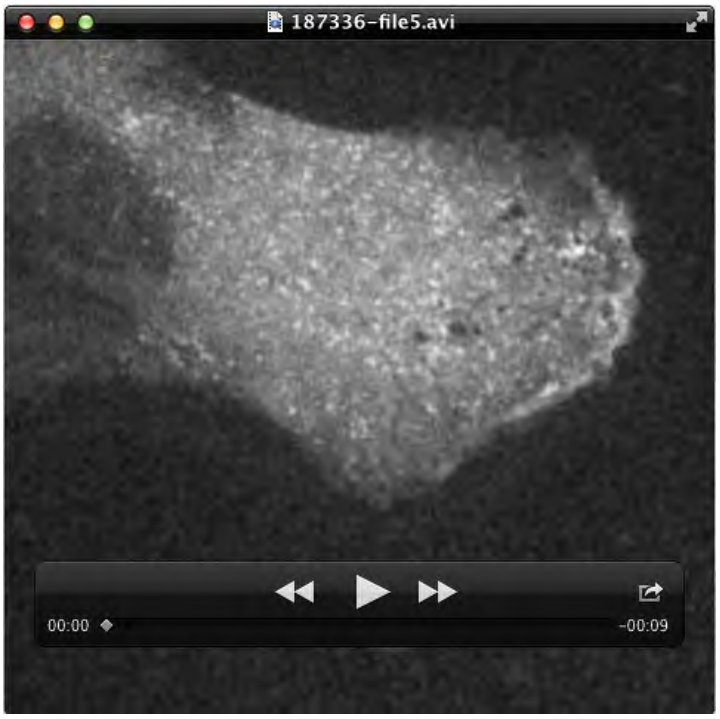

Movie 3. Sec6 dynamics in a motile cell. A HEK-HT cell, stably expressing GFP-Sec6, was visualized for 5 min (1 frame/2 s) by confocal spinning-disk microscopy.

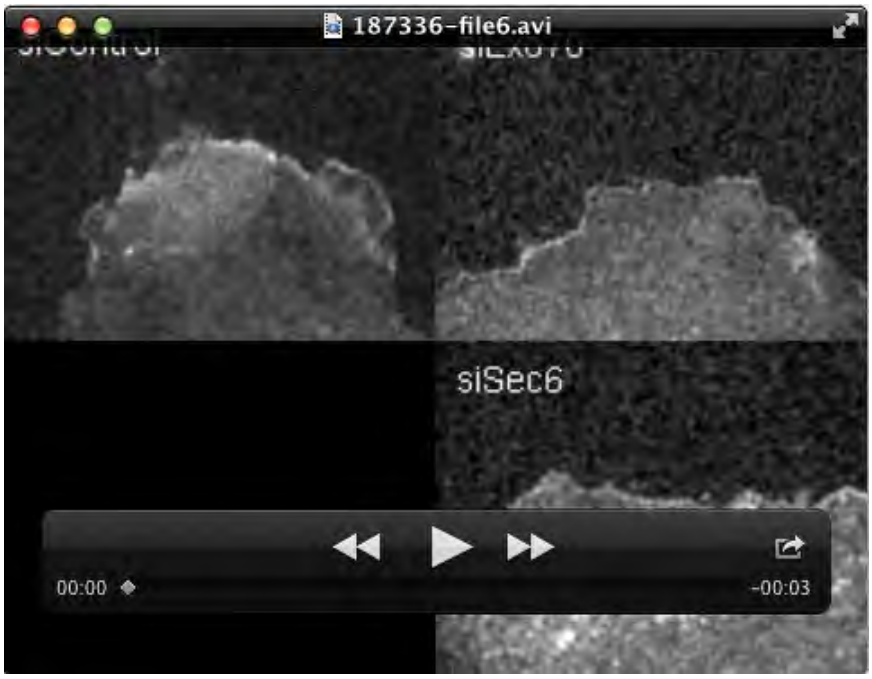

Movie 4. Effect of depletion of Sec6 or Exo70 on WRC recruitment and cell edge velocity. Representative confocal spinning-disk movies of HEK-HT cells, expressing Cherry-Abi1, treated with siControl, siExo70 or siSec6. Duration time: 2.5 min (1 frame/2 s).

SUPPLEMENTARY TABLES

Table S1. List of cell lines used in this study

Cell line	Reference	Generation method	Selection antibiotics
293	ATCC		
HEK-HT	Hanh et al., 1999		Hygromycin + Geneticin
293 FlagHA-Abi1	Derivery et., 2009		Hygrogold (Invivogen)
293 FlagHA-Cyfip1	Derivery et., 2009		Hygrogold (Invivogen)
293 HisV5-Sec6	This work	Flp-In system (Invitrogen)	Hygrogold (Invivogen)
HEK-HT mCherry-Abi1	This work	Lentiviruses infection [1]	Hygromycin + Geneticin + Puromycin
HEK-HT GFP-Sec6	This work	Retroviruses infection [2]	Hygromycin + Geneticin + Zeocin

[1] 293T cells were transfected by Lipofectamine 2000 (Invitrogen) with pLVXW-mCherry-Abi1_6 viral vector along with lentiviral packaging plasmid (psPAX2) and VSVG expression vector (pCMV-VSV-G).

[2] 293TV cells were transfected by Fugene6 (Promega) with pBabe-zeo-GFP-Sec6 viral vector along with retrovirus packaging plasmid (pCL-10A1).

Table S2. List of plasmids used in this study

Plasmid
pEGFP-Abi1_6 (transcript variant 6, 480 aa)
pEGFP-Abi1_8 (transcript variant 8, 446 aa)
pEGFP-Abi1_8-ΔN (aa 146-446)
pEGFP-Abi1_8-Y32E
pEGFP-Abi1_8-Q56A
pEGFP-Abi1_8-Y63E
pEGFP-Abi2-Nter (aa 3-147)
pEGFP-Exo70-2M (transcript variant 2), kindly provided by Dr. Wei Guo
pEGFP-Exo70-5E (transcript variant 5), kindly provided by Dr. Wei Guo
pcDNA-Exo70-HA
pcDNA-Exo70-Δ84-HA (aa 85-697)
pcDNA-Exo70-Cter-HA (aa 415-697)
pcDNA-Exo70-Nter-HA (aa 1-414)
pcDNA-mCherry-Exo70-HA
pcDNA-mCherry-Exo70-Δ84-HA (aa 85-697)
pGEF2t-Eps8-SH3 (aa 535-821, murine form)
pGEF2t-Eps8-Cter (aa 648-821, murine form)
pCXN2-mRFP-Rac1-V12
pLVXW-mCherry-Abi1_6
pBabe-zeo-GFP-Sec6

Unless specified, the genes are human.

Table S3. List of siRNAs used in this study

siRNA	Target	Sequence
siControl	No target	ON-TARGETplus Non-targeting siRNA#1 (Thermo Scientific)
siLuciferase	Luciferase	CGUACGCGGAAUACUUCGAdTdT
siRalA-II	RALA	GACAGGUUUCUGUAGAAGAdTdT
siRalB-107	RALB	UGACGAGUUUGUAGAAGACdTdT
siSec5-918	EXOC2 (Sec5)	GGUCGGAAAGACAAGGCAGdTdT
siSec5-1022	EXOC2 (Sec5)	GGGUGAUUAUGAUGUUGUGGUU
siSec6L1-31	EXOC3 (Sec6)	CACCGUGGAAGACUAUUUCAAdTdT
siExo84-1439	EXOC8 (Exo84)	CCACUUUACUCUAUAUUCAdTdT
siEXOC7-72	EXOC7 (Exo70)	CCAAGAUUUCAUGAACGUCUAdTdT
siExo70-UTR	EXOC7 (Exo70)	GACUGGCGUGUCAUUGGACAGAUAAdTdT
siARPC2	ARPC2	CCAUGUAUGUUGAGUCUAdTdT

Table S4. List of antibodies used in this study

Antibody	Provider and Reference	Dilution
anti-Abi1	Homemade (G. Scita), mouse monoclonal It weakly recognizes also Abi2	WB (1:500)
anti-Adaptin	BD transduction, #610502	WB (1:1000)
anti-ARPC1A	Sigma, #HPA004334	WB (1:5000)
anti-ARPC1B	Sigma, #HPA004832	WB (1:1000)
anti-Cyfip1	Upstate, #07-531	WB (1:500)
anti-Exo70 (clone 70X13F3)	Millipore, #MABT186	WB (1:1000)
anti-Exo70 (clone 1D4)	Sigma-Aldrich, #WH0023265M1	IF (1:20)
anti-Exo84	Kindly provided by Dr. C. Yeaman, rabbit polyclonal	WB (1:500)
anti-Flag (clone M2)	Sigma-Aldrich, #F3165	WB (1:1000)
anti-GAPDH (clone 6C5)	Millipore, #MAB374	WB (1:1000)
anti-GST	Homemade, rabbit polyclonal	WB (1:1000)
anti-GFP	Homemade, rabbit polyclonal	WB (1:1000)
anti-HA (clone 3F10)	Roche, #11867423001	WB (1:1000)
anti-Myc (clone E910)	Sigma-Aldrich, #M4439	WB (1:1000)
anti-Nap	Upstate, #07-515	WB (1:500)
anti-Rac1 (clone 23A8)	Millipore, #05-389	WB (1:1000)
anti-RalA (clone 8)	BD Transduction Laboratories, #610221	WB (1:1000)
anti-RalB	Cell Signaling, #3523	WB (1:500)
anti-Sec5	Kindly provided by Dr. C. Yeaman, rabbit polyclonal	WB (1:500)
anti-Sec6 (clone 9H5)	Stressgen Bioreagents, #VAM-SV021	WB, IF (1:20)
anti-Sec8 (clone 14)	BD transduction, #610659	WB (1:500)
anti-Wave (WP1)	Homemade (A. Gautreau), rabbit polyclonal	WB (1:500), IF (1:60)